

A Study of Tailored Oriented Thin Silver Films by X-ray Diffraction

By

Lindsay N. Timian

A thesis submitted in partial fulfillment of the requirements for
the degree of

Bachelor of Science

Houghton College

May 2010

Signature of Author

Department of Physics
May 17, 2010

.....
Dr. Brandon Hoffman
Assistant Professor of Physics
Research Supervisor

.....
Dr. Mark Yuly
Professor of Physics

A Study of Tailored Oriented Thin Silver Films by X-ray Diffraction

By

Lindsay N. Timian

Submitted to the Houghton College Department of Physics

on May 17, 2010 in partial fulfillment of the requirement for

the degree of Bachelor of Science

Abstract

The transition of crystal orientations in tailored oriented thin silver films were studied; specifically, the transition from fcc(111) to fcc(100) orientations of films ranging in thickness from 1 nm to 1000 nm. The films were deposited via electron beam evaporation onto a silicon substrate in a high vacuum chamber and passivated through sputter deposition. After thickness measurements were taken they were annealed for various times and temperatures. Putting an adhesion promoter layer of titanium on both sides of a thin film of silver sharpened the transition of silver grains between the 111 and 100 orientations. The titanium layer was deposited with a thickness gradient, to determine the thickness at which the adhesive properties of titanium took effect. Also, the percentage of the film's volume that transitioned to fcc(100) increased with anneal temperature and time.

Thesis Supervisor: Dr. Brandon Hoffman

Title: Assistant Professor of Physics

TABLE OF CONTENTS

TABLE OF FIGURES 6

Chapter 1 BACKGROUND AND MOTIVATION7

1.1 Introduction.....7

 1.1.1 History 7

 1.1.2 Motivation 7

1.2 Experiment 8

 1.2.1 Methods of Deposition 8

 1.2.1.1 Evaporative Deposition 8

 1.2.1.2 Sputter Deposition..... 9

 1.2.2 Analysis..... 9

Chapter 2 THEORY 10

2.1 Introduction..... 10

2.2 Silver Film Characteristics 10

 2.2.1 Crystal Structure.....10

 2.2.1.1 Miller Indices 11

 2.2.1.2 Silver Structure and Orientations 12

 2.2.2 Stress and Strain..... 12

2.3 Existing Model 14

 2.3.1 Dependence on Energy14

 2.3.2 Carl Thompson’s Model.....16

2.4 Film Development 17

 2.4.1 Evaporation Deposition.....17

 2.4.2 Sputter Deposition17

2.5 X-Ray Diffraction 18

2.5.1	Wave Interference	18
2.5.2	Orientation Identification	20
2.5.3	Correction Factor	21
2.5.3.1	Structure Factor	22
2.5.3.2	Area Intensity Factor.....	25
Chapter 3 DESCRIPTIONS OF APPARATUS.....		27
3.1	Overview	27
3.2	Deposition Chamber	27
3.2.1	Shutters	28
3.2.2	Ion Gun and Ion Gauge.....	29
3.2.3	Evaporation System.....	29
3.3	Profilometer.....	31
3.4	Annealing Furnace	31
3.5	Passivation Chamber	33
3.6	X-Ray Diffractometer.....	34
Chapter 4 PROCEDURE		36
4.1	Deposition Process	36
4.1.1	Ion cleaning	37
4.1.2	Film Deposition Processes	37
4.1.2.1	Films with Silver	37
4.1.2.2	Films with Silver and Titanium.....	37
4.1.2.3	Silver and Titanium with Two Gradients	39
4.2	Profilometry	39
4.3	Passivation.....	40
4.4	Annealing	41
4.5	X-Ray Diffraction	42
Chapter 5 ANALYSIS AND RESULTS.....		44
5.1	Introduction.....	44
5.2	Preliminary Results.....	44
5.3	Titanium Effects	45
5.4	Annealing Effects	46

5.4.1	Annealing Temperature	47
5.4.2	Annealing Time	48
Chapter 6 CONCLUSIONS.....		50
6.1	Summary	50
6.2	Further Analysis.....	50
6.3	Imaging.....	51
REFERENCES.....		52

TABLE OF FIGURES

<i>Figure 1. One crystal made up of three individual grains.....</i>	10
<i>Figure 2. Plane designation by Miller indices</i>	11
<i>Figure 3. The three primary orientations.....</i>	12
<i>Figure 4. Typical deposition result—film on one surface of the substrate</i>	13
<i>Figure 5. Bending due to the difference in thermal coefficients</i>	13
<i>Figure 6. Plot of total energy verses thickness.....</i>	15
<i>Figure 7. Current model for orientation behavior</i>	16
<i>Figure 8. A magnet and target for magnetron sputtering</i>	18
<i>Figure 9. Diffraction of x-rays.....</i>	20
<i>Figure 10. X-ray scattering off of electrons in an atom</i>	22
<i>Figure 11. The effect of atom position on the phase difference between diffracted x-rays</i>	23
<i>Figure 12. Diagram of Deposition Chamber</i>	28
<i>Figure 13. Diagram of ion gun</i>	30
<i>Figure 14. The evaporation system diagram</i>	30
<i>Figure 15. Diagram of profilometer</i>	32
<i>Figure 16. Diagram of Annealing Furnace.....</i>	33
<i>Figure 17. Sputtering chamber used to passivate samples.....</i>	34
<i>Figure 18. Scintag X-ray Diffractometer</i>	35
<i>Figure 19. Silicon substrate with metal strip placed down center</i>	36
<i>Figure 20. Diagram represents a silver film with a thickness gradient.....</i>	38
<i>Figure 21. Silver gradient with half titanium</i>	38
<i>Figure 22. Silver and titanium with perpendicular gradients.....</i>	39
<i>Figure 23. The diffractometer sample holder</i>	42
<i>Figure 24. Preliminary data plot of a silver film.....</i>	44
<i>Figure 25. Comparison of film data that has titanium layers of various thicknesses.....</i>	45
<i>Figure 26. Analysis of sample pre-passivation and pre-anneal.....</i>	46
<i>Figure 27. Silver film without titanium layers annealed for 1 hour at varying temperature</i>	47
<i>Figure 28. Silver film with titanium layers annealed for 1 hour at varying temperatures</i>	48
<i>Figure 29. Silver films with titanium layers annealed for increasing periods of time.....</i>	49

Chapter 1

BACKGROUND AND MOTIVATION

1.1 Introduction

1.1.1 History

At the beginning of the 21st century, the United States National Academy of Engineering revealed the results of a study which identified the twenty greatest engineering achievements of the previous century. The accomplishments were in a variety of areas, such as electronics, computers, health technologies and optics, but each was based on the advances of material technology and thin film technology represented a significant component of that development [1]. Thus, the applications of thin films lie in multiple areas of science and technology. To exemplify, thin films are used in optics as reflective or antireflective coatings, interference filters or as decoration. In electronics, films are used in semiconductor devices and as conductors or inductors [2]. As the dimensions of electronic devices decrease, the thickness of the metal layers used in such devices should decrease, but the decrease in thickness of thin films changes the electrical properties as well as the microstructures [3].

1.1.2 Motivation

The properties of a thin film are different from when the material is in its bulk form [4]. This had led to research, to determine some of the new properties. In discovering new properties of thin films, new uses for those films are developed. Specifically, the mechanical properties of metallic thin films have been extensively studied because of the technological applications, in photovoltaics and DVD's or optical devices. [3,5,6,7]. One such property is when films are deposited on rigid surfaces and exposed to thermal changes the difference in thermal coefficients causes thermal stress. These stresses are often higher than the typical stresses developed in bulk metals, and thus the film can have questionable reliability [8]. Knowing the point at which the internal stresses cause the film to break down would aid in constructing films and thereby devices, such as the ones listed above, that are not susceptible to failure.

Specifically, thin silver films have been found to be the most thermally and electrically conductive, when compared with other common films such as copper or aluminum. Silver also excels at resisting

two of the causes of material failure, namely oxidation and electromigration. Electromigration is the change that takes place in a film when atoms in the material shift because of high current densities. Silver is preferred for applications of ultra-large scale integration (ULSI) technology because of its high electromigration resistance [3]. The properties inherent in silver allow the applications of thin films to be more stable, thereby making thin silver films a valuable area of research.

1.2 Experiment

In this experimental research, films that demonstrated the orientation transition, between fcc(100) and fcc(111), are deposited and studied. The orientation of a thin film influences the properties of the film, which makes it an important factor to determine [9]. Films of silver are made, as well as films that have layers of titanium on either side of the silver film. The films are deposited in a thickness gradient across the substrate so that data can be acquired for various thicknesses. As thickness increases the films transition from (111) to (100) orientations and titanium, an adhesion promoter, appears to sharpen that transition. The films are annealed and each sample piece of film is analyzed with x-ray diffraction to determine the percent (111) orientation. The resulting data is plotted versus thickness so that the resulting transition of each film could be observed. Thus, before the orientations can be studied the thin films must be made and the two methods of film deposition used in this experiment are described as follows.

1.2.1 Methods of Deposition

The two primary methods of building a film atomically are chemical vapor deposition (CVD) and physical vapor deposition (PVD). If there is a chemical reaction that causes a vapor of atoms, then it is a CVD method [10]. If the vapor is created physically, without a chemical reaction, then it is classified as PVD. Within PVD there are two common techniques, evaporative and sputter deposition. These two methods of deposition are the only techniques used to make films in this experimental process.

1.2.1.1 Evaporative Deposition

In this experiment, evaporative deposition is used to deposit silver and titanium (see Figure 12 for the diagram of the high vacuum evaporation chamber). In general, the metal source, while in crucibles, may be heated via resistance heating, high frequency induction heating or electron beam evaporation.

After being heated the source will sublime. The evaporated atoms will proceed to travel through the pressurized chamber and condense on the substrate [10]. The material is generally an appreciable distance away from the substrate to promote evenly distributed deposition layers and to prevent radiant heating of the deposition surface. Vacuum deposition is often used to form protective, optical interference and mirror coatings [11].

1.2.1.2 Sputter Deposition

In reactive sputter deposition, ions of gas are accelerated by an imposed electrical field to strike an elemental source. The ionized gas is typically one of two types; either an Argon-Nitrogen, Argon-Oxygen mixture, or pure Argon is used for inert gas sputtering. The ensuing transfer of momentum causes the neutral atoms of the source to dislodge, creating a vapor in the chamber (see Figure 17). The vapor of particles moves through the ionized gas and, upon contact with the substrate, yields film growth [11]. Films are made through sputter deposition for uses such as reflective coatings on compact discs, dry film lubricants or decorative coatings [11]. In this experiment only the passivation layer, which is placed on top of the silver or titanium film is deposited via sputter deposition.

1.2.2 Analysis

The primary method of determining the crystalline structure and characteristics of a film is through x-ray diffraction. Given that this is the information being studied, each film is analyzed via x-ray diffraction. The diffractometer functions by directing x-rays at a film over a range of angles, where the x-rays reflect off of the film and are counted by an x-ray detector. The number of x-rays for a given angle can be related to the quantity of atoms in the film that are in a specific orientation; therefore, the comparison of the counts from the diffraction data yields the relative volume of the orientations in the film.

Chapter 2

THEORY

2.1 Introduction

In this chapter the theory of film orientations and deposition processes to make such films are discussed. The characteristics of silver crystals determine the energy in the film, which influences the orientations. Thus, establishing the properties of a silver film structure can aid in determining why the film has a particular orientation. The orientations of the film, for a given thickness, can be determined through x-ray diffraction, which applies the principles of constructive interference and Bragg's law.

2.2 Silver Film Characteristics

2.2.1 Crystal Structure

A crystal is a solid that has grains, where grains are made up of unit cells. Unit cells are individual molecular structures that are identical to each other. Thus unit cells form a repeatable pattern, and a collection of these periodic structures is called a grain. Any crystal can be made up of either a single grain or multiple grains.

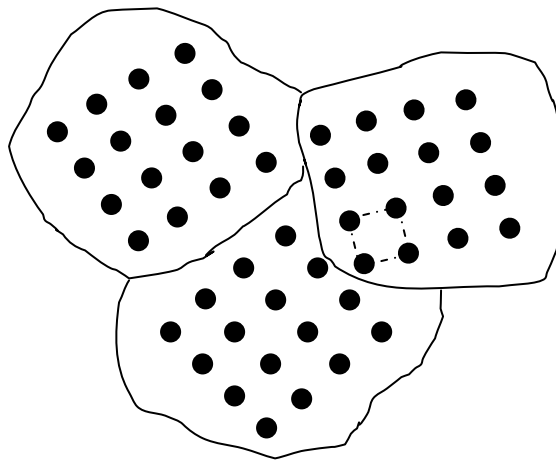


Figure 1. Shown here is one crystal made up of three individual grains. Within each grain there is a repeatable structure of atoms (the black dots) that make up the unit cells. An individual unit cell is denoted by the dashed line within the grain on the right.

2.2.1.1 Miller Indices

A significant area of crystallography is the study of the relative orientations of the grains within the crystal lattice structure. The grains in a crystal may look identical to or very different from each other; their appearance varies considerably with the conditions of growth, but regardless of the shapes of the grains the angles between the corresponding faces of the unit cells remains constant [12]; meaning the unit cell within the grain will not change its shape or structure. A three dimensional crystal can be described by three vectors \mathbf{a} , \mathbf{b} , and \mathbf{c} which are not in the same plane and not necessarily perpendicular. These vectors form an ideal frame of reference, for which an arbitrary plane will intersect the line formed by each vector. These intersections will be at distances from the origin that can be defined in terms of each vector's magnitude, for example a/h . The plane is then fully defined by h , k , and l , (see Figure 2) and it should be noted that when a plane is parallel to any one of the vectors the intercept is effectively infinity. Miller indices are traditionally used to represent the specific grain orientation in the crystal, because it is difficult to use infinity as part of a definition. Miller indices are the reciprocals of the fractional intercepts which the plane makes with the vectors, multiplied by a constant so that each index is an integer value. Thus Miller indices are three integers enclosed in parenthesis, for example (111) [12].

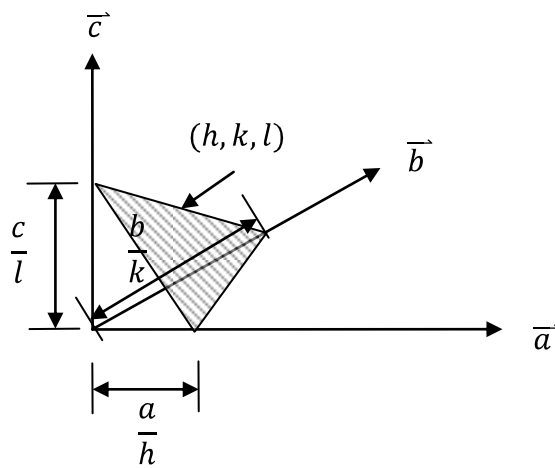


Figure 2. Plane designation by Miller indices, the vectors \mathbf{a} , \mathbf{b} , and \mathbf{c} are vectors that are used to describe a three dimensional crystal. The points at which the plane intersects the vector are defined in terms of the vector magnitude (\mathbf{a} , \mathbf{b} , \mathbf{c}) and the Miller indices (h , k , l). Note that (h, k, l) , multiplied by a constant represents the plane itself.

2.2.1.2 Silver Structure and Orientations

Looking specifically at silver, it is a face-centered cubic (fcc) crystalline molecular structure; meaning in each cubic molecule there is an atom at each corner and in the middle of each face. The preferred orientations of the crystal grains are those which have the lowest surface energy and highest packing density; for silver, the two primary orientations are (111) and (100) [13]. A film with (100) orientations contains unit cells aligned such that the highlighted side of the cubic molecule, as seen in the image on the left of Figure 3, is parallel to the substrate surface. In (111) oriented films the unit cells are aligned so that the plane on the right side of Figure 3 is parallel to the substrate surface. Note that in (200) oriented films the plane in the center figure is the one parallel to the substrate surface, and this plane is parallel to the (100) plane and the distance between the two planes can be represented by $\frac{a}{2}$.

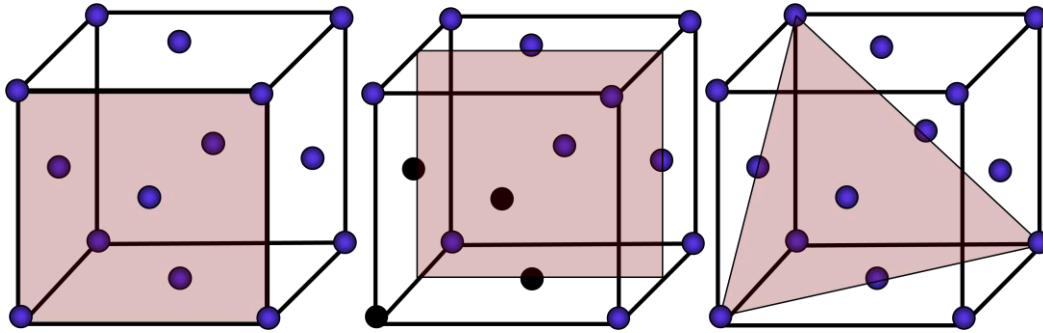


Figure 3. The (100) orientations (left), (200) orientation (center) and (111) orientation (right). All three cubes are fcc structures, with atoms at each corner and in the middle of each face. Each highlighted plane is parallel to the substrate, representing three possible orientations. The darkened atoms in the center structure are the four atoms which compose every fcc structure (which has a four atom basis).

2.2.2 Stress and Strain

To produce silver films through deposition there must be a substrate to deposit the metal on as shown in Figure 4. In most systems the film and substrate have different coefficients of thermal expansion;

therefore, when the temperature of the environment is increased, each will expand at a different rate, thereby developing different lengths.

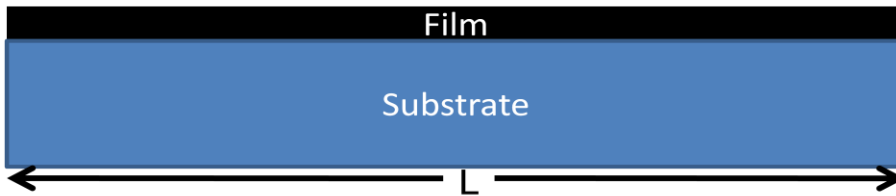


Figure 4. Typical deposition result—film on one surface of the substrate. From this diagram it can be seen that L is the original length of both the film and the substrate.

However, the film and the substrate are still attached to each other so, in order for one to be longer than the other, they curve as shown in Figure 5.

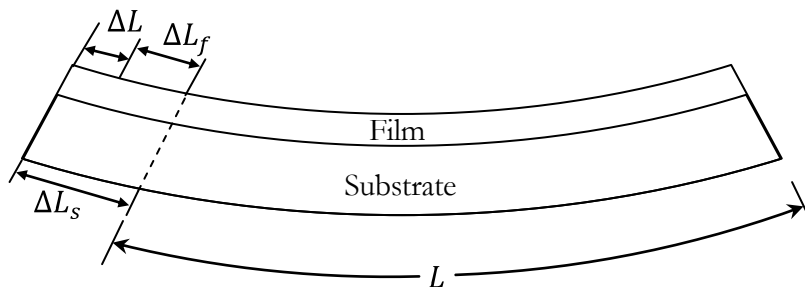


Figure 5. Bending due to the difference in thermal coefficients. Both film and substrate start with original length L , but after thermal expansion the film and substrate expand by ΔL_f and ΔL_s respectively. Because film and substrate are attached to each other the substrate forces the film to expand an additional length ΔL .

Because the materials are experiencing differing rates of expansion there is a stress induced in the film [14]. The stress occurs because the substrate has expanded by ΔL_s and the film has expanded by ΔL_f , which are the lengths each would expand if they were separate. But because they are attached to each other and must stay the same length, there is a force that the substrate applies to the film that stretches it by ΔL . This is the strain experienced by the film where strain, ε , is defined as the amount of deformation per unit length of an object when a force is applied [15]. Thus strain can be expressed with the following equation,

$$\varepsilon = \frac{\Delta L}{L}, \quad (1)$$

where L is the original length of the film. When the film undergoes a strain it experiences a change in energy which can be used to derive a model for the preferred orientations of the film, because for each orientation the film has a distinct amount of energy and any system will transition to the lowest energy state possible.

2.3 Existing Model

The model which was tested against the experimental data is based on the theories developed by Carl Thompson of MIT [16]. Thin films have preferred orientations and the following sections discuss the reasons for these preferences.

2.3.1 Dependence on Energy

From the amount of strain and interface energy in the film the orientation preference can be predicted, due to the principle of energy minimization. The sum, Φ , of the strain and interface energy in the film is

$$\Phi = \mu \cdot t_f + \gamma, \quad (2)$$

where μ is the strain energy in the film per unit volume, t_f is the thickness of the film and γ is the interface energy per unit area of the surface. The interface energy is the energy between the film and the substrate. The following two equations of inequality apply to face centered cubic metals.

$$\mu_{111} > \mu_{100} \quad (3)$$

$$\gamma_{100} > \gamma_{111} \quad (4)$$

Thus (2) can be written as for each orientation like so.

$$\Phi_{100} = \mu_{100} \cdot t_f + \gamma_{100}, \quad (5)$$

$$\Phi_{111} = \mu_{111} \cdot t_f + \gamma_{111} \quad (6)$$

equations (5) and (6) are in the form of lines, where μ is the slope of the line and γ is the Φ -intercept. Therefore, from the inequalities stated above, plotting energy versus thickness yields Figure 6.

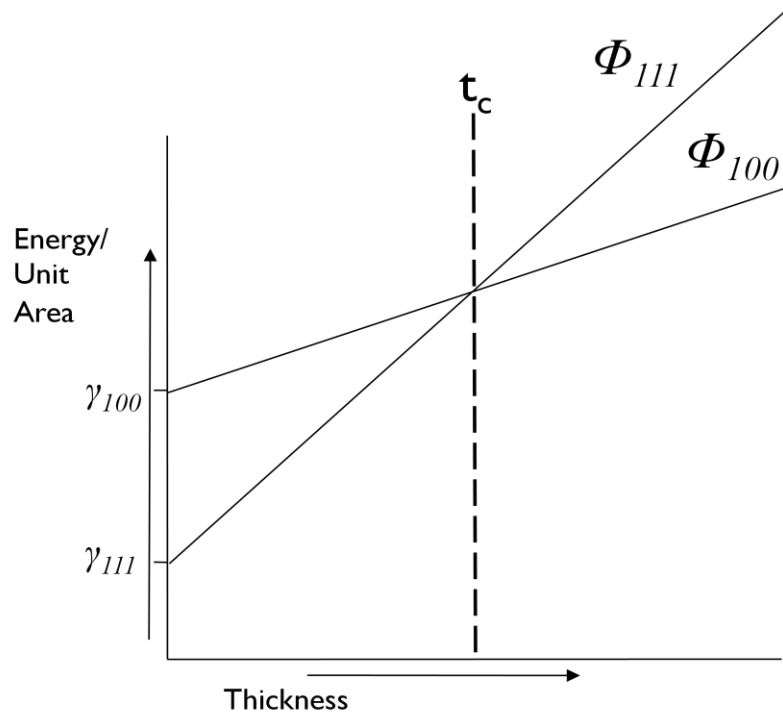


Figure 6. Plot of total energy versus thickness, where the two orientations intersect at a specific thickness t_c . Note that there is interface energy as soon as the film thickness is non-zero. But more importantly, the lower energy state is given by (111) orientations to the left of t_c and (100) orientations to the right; thus, because systems will tend towards the lowest energy state possible the preferred orientation changes with thickness.

Given that μ is less for (100) orientations than it is for (111) orientations, the slope for $\Phi_{(100)}$ is going to be less than $\Phi_{(111)}$; thus, the two lines will intersect each other. The thickness at this point of intersection is defined as the critical thickness, t_c . All physical systems tend toward the lowest energy state possible. Thus for films with thickness $t_f < t_c$, the (111) orientation will be favored. After the film thickness reaches t_c , the (100) orientation will be the state of lower total energy. This leads to the development of a model of silver orientation behavior.

2.3.2 Carl Thompson's Model

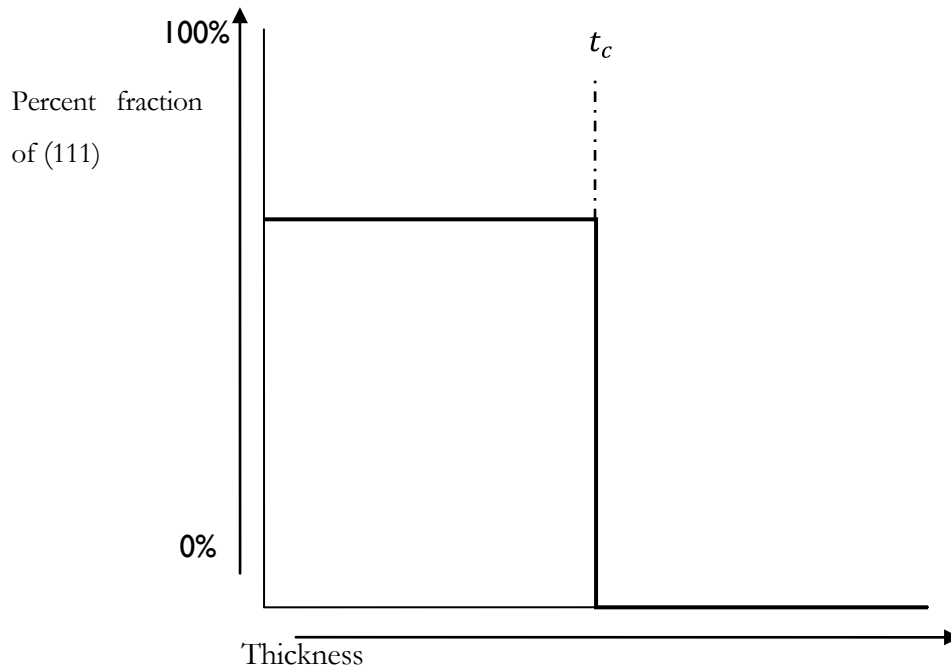


Figure 7. Current model for orientation behavior, based on Carl Thompson's theory of energy minimization. This model diagrams a clearly defined point of grain orientation transition. Film that has thickness less than the critical thickness will be completely (111) orientation and film that has greater will be completely (100) orientation.

According to this model the silver grains in a film will maintain a (111) orientation until they reach t_c , at which point they will transition into (100) oriented grains. Prior research showed the orientation transition of silver films to be more gradual than what this model predicts [17]. The aforementioned

data indicates that depositing layers of Ti, which is an adhesion promoter, on either side of the silver film creates films in which the transition is sharper.

2.4 Film Development

In order to have experimental data, films must be deposited for ensuing analysis. This section discusses the two systems that were used to deposit films in this experiment.

2.4.1 Evaporation Deposition

All of the silver and titanium films are deposited through evaporation. Electrons thermionically emitted from a hot filament and accelerated into the source material can generate enough energy density to evaporate any material [18], as shown in Figure 14. The evaporation system that is used has an evaporation hearth that includes a focused electron beam, where the electrons are emitted from a hot filament placed below the hearth. This prohibits interference between the evaporated particles and the filament (emitting the electron beam). The combined force, F , on an electron in electric and magnetic fields is given by the Lorentz force equation [18]:

$$\mathbf{F} = \mathbf{F}_E + \mathbf{F}_B = q_e \mathbf{E} + q_e \mathbf{v} \times \mathbf{B}. \quad (7)$$

The first force term accelerates the electrons away from the filament thereby giving them a velocity component. Due to the cross product in the second term, the emitted electrons will be directed in a circular path that can be focused directly onto the source metal. The magnetic field is generated by permanent magnets placed inside the hearth.

2.4.2 Sputter Deposition

The method of sputter deposition is used to passivate the silver and titanium films. The chamber used for passivation is a DC magnetron sputtering system. For magnetron sputtering, the chamber is pressurized with Argon gas at 4 mtorr and a large negative voltage of ~ 147 V applied to the target. This high voltage applied to the target material gives the electrons in the target material enough energy to break free. These electrons interact with the Argon gas, thus ionizing it, which produces secondary electrons and creates plasma. The positively charged Argon ions are then attracted to the negatively charged target source and by momentum transfer free the source particles, which will condense on the substrate, as diagramed in Figure 17. The placement of a magnet near the target as shown in Figure 8

keeps the secondary electrons localized and thus sustains the plasma. The electrons, traveling with some arbitrary velocity and direction, will experience a force due to the magnetic field and will subsequently follow a circular path (as detailed in the previous section) perpendicular about the magnetic field lines. In the absence of an electric field, the circular path of an electron initially moving in an arbitrary direction (with respect to the magnetic field) for a system set up like the diagram (Figure 8), will spiral around the magnetic field line, due to the initial component of velocity that is parallel to the field line. In the presence of an electric field there is an additional component of acceleration away from the magnet. The fact that the electrons are moving in a spiral about the magnetic field is beneficial because it provides more opportunity for the secondary electrons to collide with an Argon atom, thereby ionizing it, and also because it reduces the possibility of contamination of the film by keeping the plasma close to the target.

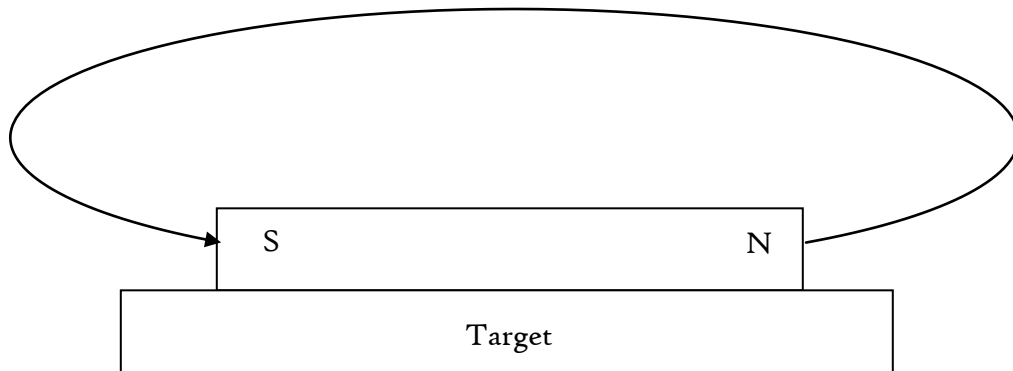


Figure 8. A magnet placed near the target will produce a magnetic field about which the secondary electrons will spiral. The magnet thus sustains the plasma by keeping the electrons circulating (within the Argon gas) which increases the chance of a collision and ionization of the Argon which, once positively ionized, is then accelerated towards the negatively charged target.

2.5 X-Ray Diffraction

2.5.1 Wave Interference

X-ray diffraction can be used to determine the crystalline orientations of the thin film being analyzed and diffraction involves wave interference. Thus, the property of wave interference will be discussed

in this section. For any wave of wavelength, λ , the path length from one position to another in one dimension is defined as x . For two waves with different paths, the path length difference is simply the difference in their respective x values. The phase, ϕ , of a wave can be expressed in terms of the path length by the following relation:

$$\phi = \frac{2\pi x}{\lambda}. \quad (8)$$

The time independent form of the equation for a wave is

$$\psi = f e^{i\phi}, \quad (9)$$

where f is the amplitude of the wave. When two waves with equal frequency and amplitude interfere, their wave functions can be superimposed, and summed as follows.

$$\psi = f e^{i\phi_1} + f e^{i\phi_2}, \quad (10)$$

$$\psi = f e^{i\phi_1} (1 + e^{i\Delta\phi}), \quad (11)$$

where the phase difference is defined as $\Delta\phi = \phi_2 - \phi_1$. The intensity is equivalent to the amplitude squared, so

$$|\psi|^2 = f^2 |1 + e^{i\Delta\phi}|^2, \quad (12)$$

$$|\psi|^2 = f^2 (2 + e^{i\Delta\phi} + e^{-i\Delta\phi}), \quad (13)$$

$$|\psi|^2 = 2f^2 (1 + \cos \Delta\phi), \quad (14)$$

because $\cos \Delta\phi = \frac{e^{i\Delta\phi} + e^{-i\Delta\phi}}{2}$. Note that when the phase shift is the same for both waves, the intensity is increased because then the cosine term becomes one and the amplitude is $2f$; therefore, the intensity equals $4f^2$. This relation between phase shift and intensity applies to all scattered waves.

2.5.2 Orientation Identification

Before addressing how the intensity of scattered waves influences the quantity of a particular orientation in a film sample, the method of determining the specific orientation is described. X-ray diffraction can identify the crystalline orientations of a thin film. This is due to the fact that the atomic structure of a crystal diffracts x-rays. B.D. Cullity defines a diffracted beam as a beam composed of a large number of scattered rays mutually reinforcing one another [19]. Thus diffraction occurs when the x-rays reflect off of atomic planes that cause constructive or destructive interference. Constructive interference is when superimposed waves result in increased amplitude. Similarly, destructive interference is when the amplitude is decreased. The condition for constructive interference is when the path length difference between the waves, $2 \cdot d \cdot \sin(\theta)$ as shown in Figure 9, is equal to a whole number n of the wave length, λ , of the x-ray beams [19]. Then when the two incoming waves are initially in phase the following equation, known as Bragg's law, holds true.

$$n\lambda = 2 \cdot d \cdot \sin(\theta) \quad (15)$$

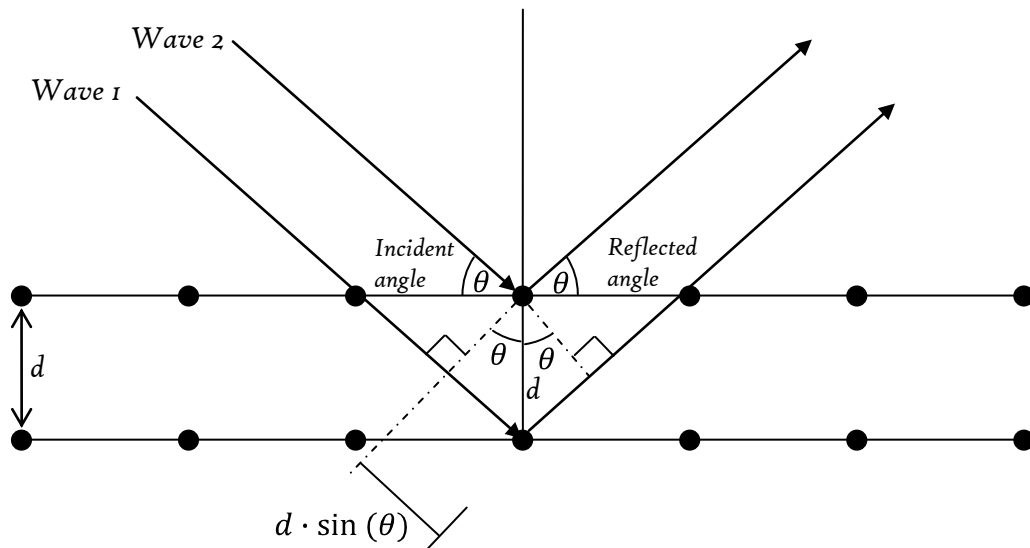


Figure 9. Diffraction of x-rays, denoted as Wave 1 and 2, by a crystal lattice with atomic spacing, d . The path length difference for this situation is given by $d \sin \theta$, as shown in the diagram.

For polycrystalline films, the degree of preferred orientation is found through a 2θ or Bragg-Brentano scan. The film is set in horizontal plane and θ is measured from the horizontal. The x-rays are projected at the incident angle θ and detected at the reflected angle θ while the scan is taken over a range of angles of θ . At values of 2θ for which the atomic periodicity d perpendicular to the film surface satisfies the Bragg condition for the given λ , constructive interference occurs, yielding a measurable intensity of x-rays from which d , and thus the orientation can be determined [20]. That value identifies the specific atomic plane and thus the orientation of the crystals in the film; the intensity of the reflected x-rays is relative to the number of crystals that have that specified orientation. The data from a 2θ x-ray diffraction scan can be used to calculate the relative volume of (100) or (111) orientations in a thin silver film, as detailed in the following sections.

2.5.3 Correction Factor

The x-ray detector in the diffractometer counts the number of x-rays reflected at a given angle and the intensity measured by counts can be integrated over a range of angles to yield an integrated intensity (I_{int}) value. The desired data is the relative volume of specific orientations which is proportional to the number of atoms which is proportional to the number of counts. Thus the relative volume can be determined from the integrated intensity.

The integrated intensity is complicated by the fact that waves scatter off of multiple electrons in an atom. Also the atomic structure of a particular orientation must be taken into account by a factor that compensates for its structure. Therefore, the integrated intensity depends on the number of atoms in a specific orientation (N_{hkl}), the structure factor of that orientation (F_{hkl}), and the area of the intensity peak (A_{int}), or $I_{int} \propto N_{hkl}F_{hkl}A_{int}$. Therefore,

$$N_{hkl} \propto \frac{I_{int}}{F_{hkl} \cdot A_{int}}. \quad (16)$$

Thus in order to determine the correct number of atoms, the I_{int} obtained directly from the diffractometer must be divided by a correction factor, defined as $F_{hkl} \cdot A_{int}$. The two components of the correction factor are derived in the following sections.

2.5.3.1 Structure Factor

The structure factor applies to any sample being analyzed with scattered x-rays. When x-rays diffract off of electrons in one atom, the path length difference between the waves scattered off two electrons increases as $\sin \theta$; see Figure 10.

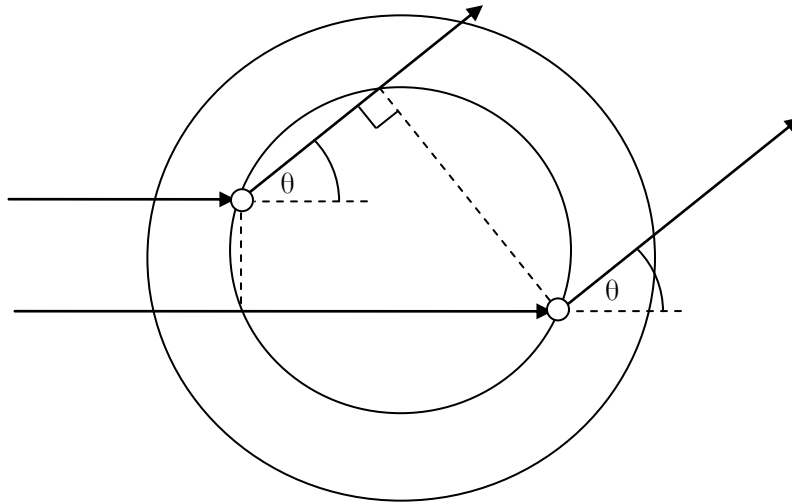


Figure 10. X-ray scattering off of electrons in an atom. The x-rays come in from the right and are scattered at angles of theta off of the electrons in the atom.

The phase between the waves increases as the path length over the wavelength, from (8). Thus, from section 2.5.1, the amplitude decreases as $\frac{\sin \theta}{\lambda}$. Therefore, different angles will yield different amplitudes. Thus each atom in a given orientation will have an amplitude of f , defined as the scattering factor, which are $f_{(111)} = 37.45$ and $f_{(200)} = 35.51$. Note that the need for a scattering factor of the (200) plane is apparent at the end of the section. The structure factor takes into account each atom in the unit cell, so the intensity due to all the atoms in a periodic structure is derived following the same method as in the beginning of this chapter.

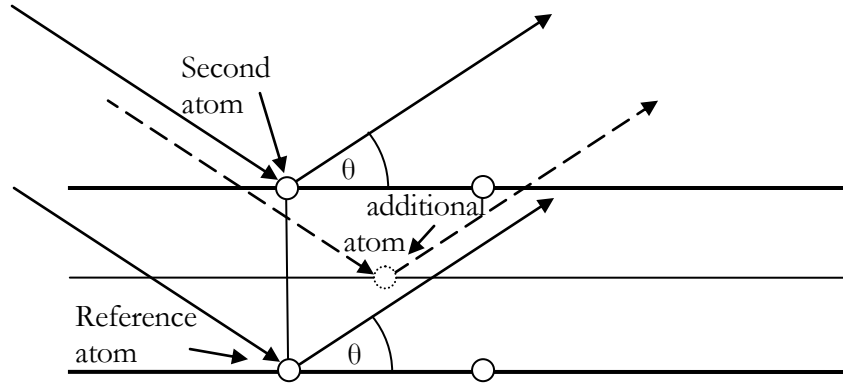


Figure 11. The effect of atom position on the phase difference between diffracted x-rays. For a given atom placed at the origin of a unit cell (Reference atom) and another atom at the origin of a second unit cell (Second atom) the waves will be reflected as shown and the path length difference can be observed as being proportional to $\sin \theta$. The path length difference between the reference atom and any other atom in the unit cell can be expressed in terms of the original path length difference.

The phase difference between the reference atom, set at the origin of the coordinate system, and any other atom in the unit cell can be derived [21]. So first take the generic equation for phase:

$$\phi = \frac{2\pi}{\lambda} x. \quad (17)$$

Then suppose Bragg's law is met (for the first order, $n = 1$ case) for the reference atom and a second atom which is at the origin of the adjacent unit cell, where d , from the definition of Miller indices, is defined as $\frac{a}{h}$. Thus the path length difference between x-rays scattered off of reference atoms of adjacent cells, δ_{cell} , is defined as:

$$\lambda = \frac{2a}{h} \sin \theta \equiv \delta_{cell}. \quad (18)$$

However, there may be an additional atom (labeled in Figure 11) that lies elsewhere in the unit cell, between the two original atoms. For any additional atom in the unit cell, the ratio of the path length differences of this partial cell is equivalent to the ratio of the d values:

$$\frac{\delta_{partial}}{\delta_{cell}} = \frac{d_{partial}}{d_{cell}} = \frac{d_{partial}}{\frac{a}{h}}. \quad (19)$$

Therefore, defining $d_{p,a}$ as $d_{partial}$ in the \vec{a} direction, the path length difference between any two atoms in the cell can be expressed as,

$$\delta_{partial} = \frac{d_{p,a}h}{a}, \quad \delta_{cell} = \frac{d_{p,a}h}{a}\lambda. \quad (20)$$

Then the phase difference between the reference atom and any other atom can be written in terms of the path length difference,

$$\Delta\phi = \frac{2\pi}{\lambda} \left(\frac{xh\lambda}{a} \right) = \frac{2\pi xh}{a}, \quad (21)$$

because the reference atom is position zero. Define the fractional coordinate as $\frac{d_{p,a}}{a} = u$; therefore,

$$\Delta\phi = 2\pi hu. \quad (22)$$

Applying this to three dimensions, let $\frac{d_{p,b}}{b} = v$ and $\frac{d_{p,c}}{c} = w$, where $d_{p,b}$ and $d_{p,c}$ represent $d_{partial}$ in the \vec{b} and \vec{c} directions respectively. This leads to the following:

$$\Delta\phi = 2\pi(hu + kv + lw). \quad (23)$$

Thus the general form of a wave can be written as,

$$Ae^{i\Delta\phi} = fe^{2\pi i(hu+kv+lw)}. \quad (24)$$

Since the scattering factor can be expressed as the total intensity of the resultant wave scattered from N atoms in the unit cell, F_{hkl} can be found through the total amplitude squared. The total amplitude (of the resultant wave scattered from N atoms in the unit cell) is expressed generally by the following sum:

$$A_{hkl} = \sum_1^N f_n e^{2\pi i(hu+kv+lw)}. \quad (25)$$

However, silver being fcc, is composed of four atoms that form its periodic structure; see Figure 3. So for the fcc case where the four highlighted atoms have (u, v, w) coordinates of (000) , $(\frac{1}{2}, \frac{1}{2}, 0)$, $(\frac{1}{2}, 0, \frac{1}{2})$ and $(0, \frac{1}{2}, \frac{1}{2})$, the intensity of the total scattering factor is

$$F_{hkl} = |A_{hkl}|^2 = \left(f e^{2\pi i(0)} + f e^{2\pi i(\frac{h}{2} + \frac{k}{2})} + f e^{2\pi i(\frac{h}{2} + \frac{l}{2})} + f e^{2\pi i(\frac{k}{2} + \frac{l}{2})} \right)^2, \quad (26)$$

$$F_{hkl} = \left[f \left(1 + e^{\pi i(\frac{h}{2} + \frac{k}{2})} + e^{\pi i(\frac{h}{2} + \frac{l}{2})} + e^{\pi i(\frac{k}{2} + \frac{l}{2})} \right) \right]^2. \quad (27)$$

So for the two orientations of concern, $|A_{(111)}|^2 = 16f_{(111)}^2$, and $|A_{100}|^2 = 0$. Therefore, no intensity would be detected at an angle θ that corresponds to a plane spacing where $d = a$. However note that $|A_{(200)}|^2 = 16f_{(200)}^2$ and this is the same orientation of the (100) plane. For this reason, scattering intensities from the (111) and (200) planes are used for comparison of the two primary orientations. Thus the F_{hkl} part of the correction factor is determined. Once the A_{int} factor is established, the correction factor to find the correct number of atoms in each orientation can be used to find the relative volume of each orientation in the sample.

2.5.3.2 Area Intensity Factor

Intensity is non-zero over a range of angles, therefore it is useful to integrate the intensity over that range to detect the reflected x-rays over the entire surface area of the sample. For a particular peak diffraction angle θ , the area of the integrated intensity depends on the maximum intensity, I_{max} , and

the breadth, or range of $\Delta\theta$ about the peak θ . I_{max} is proportional to $\frac{1}{\sin\theta}$ and $\Delta\theta$ is proportional to $\frac{1}{\cos\theta}$. Thus

$$A_{int} \propto \frac{1}{(\sin\theta \cos\theta)} \propto \frac{1}{\sin 2\theta}. \quad (28)$$

Therefore, recalling $N_{(hkl)}$ as the number of atoms of a specific orientation in the sample, it can now be expressed as the following proportion:

$$N_{(hkl)} \propto \frac{I_{int}}{16f_{(hkl)}^2 \cdot \frac{1}{\sin(2\theta)}}. \quad (29)$$

Since the volume of the film that has particular orientation, $V_{(hkl)}$, which is proportional to $N_{(hkl)}$, then

$$V_{(hkl)} \propto \frac{I_{int}}{16f_{(hkl)}^2 \cdot \frac{1}{\sin(2\theta)}}. \quad (30)$$

Finally to find the relative volume percent of (111) apply the following equation:

$$\%(111) = \frac{V_{(111)}}{V_{(111)} + V_{(200)}} \cdot 100. \quad (31)$$

This percent value is then plotted versus the film thickness to obtain the desired plots for analysis.

Chapter 3

DESCRIPTIONS OF APPARATUS

3.1 Overview

This chapter details the specific descriptions of each apparatus used and its relation to the experimental process. It begins with the high vacuum deposition chamber, in which the key internal components are detailed. Then the apparatus used to measure the thickness of the thin film is described, followed by the passivation and annealing chambers. The final section explains the x-ray diffractometer used to analyze the films.

3.2 Deposition Chamber

The chamber used to deposit the films is in Figure 12. This chamber is located at the Cornell Center for Materials Research (CCMR) department, and is currently able to consistently pump down to $\sim 10^{-6}$ torr.

This chamber is designed so that the upper part can be raised when not under vacuum, and the interior of the chamber be accessed easily. The upper part of the chamber contains the components that hold and rotate the substrate during deposition. The rotary motor has one speed and can be turned on and off momentarily in order to rotate the substrate to different angles between layers of film deposition or left on to rotate continually during ion cleaning. The substrate holder is then attached to the rotary system at the top of the chamber and is centered above the evaporation system and the shutters, as shown in the diagram.

When the chamber reaches vacuum pressure less than 10^{-4} torr, the chamber pressure is measured with a hot cathode ion gauge, where a cathode filament inside the gauge produces an electron beam which ionizes the surrounding gas (inside the gauge). The ionized particles are then collected by a negatively charged electrode and the current through the electrode is measured. The current is proportional to the amount of ionization occurring and the rate of ionization depends on the pressure of the system. Therefore the calibrated ion gauge yields the vacuum level of the chamber for each deposition.

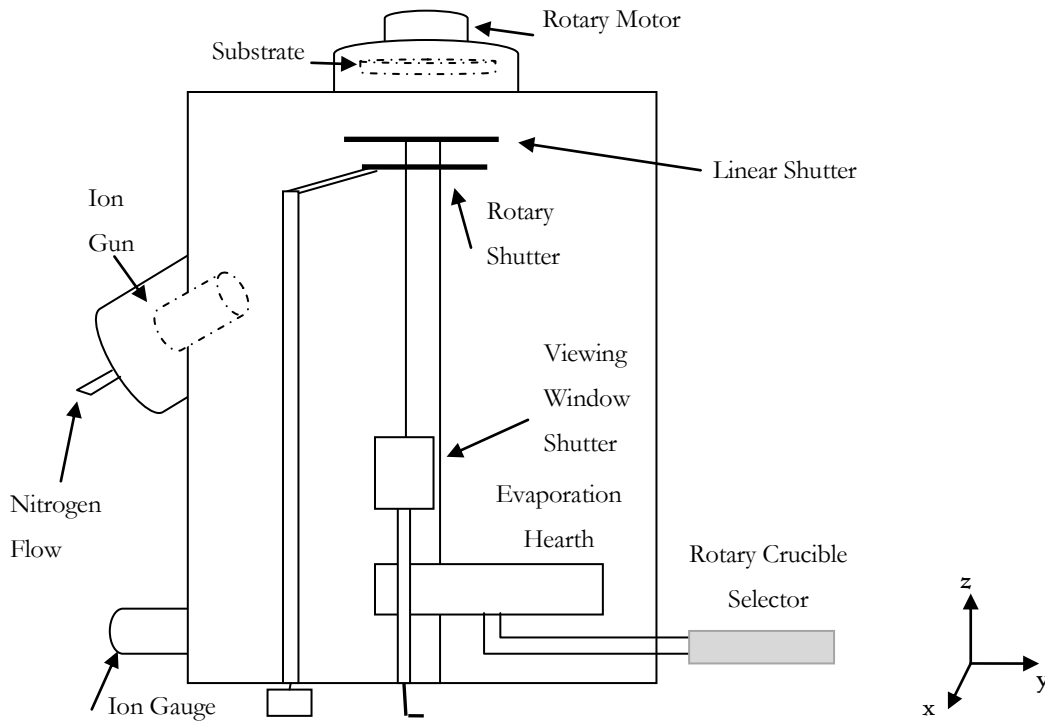


Figure 12. Diagram of Deposition Chamber. Average deposition pressure reaches $\sim 10^{-6}$ torr. The shutters in the chamber are designed to allow the substrate and viewing windows to be exposed to the evaporated particles for controlled periods of time. The evaporation hearth is in the bottom of the chamber and the substrate housing is on the top. The ion gauge and gun are on the side of the chamber so that there is no interference with the stream of evaporated particles.

3.2.1 Shutters

The shutters in the chamber work both separately and together to perform various functions of protection from the evaporated particles. The Viewing Window shutter has a handle outside the chamber that rotates the shutter about the x-axis; it is moved into place during evaporation so that the viewing window will not be covered by metal particles. The upper shutters are used to cover the substrate so that it is exposed to either the ion gun or the evaporated particles for controlled periods of time. The rotary shutter has a handle at the bottom of the chamber so that it can be also be rotated by hand about the z-axis rapidly thereby enabling a relatively instantaneous transition between exposure

and protection. The linear shutter is connected to a programmable motor, which enables the films to be deposited with a thickness gradient.

3.2.2 Ion Gun and Ion Gauge

The ion gun, as shown in Figure 13, used to clean off atmospheric contamination before deposition, is located on the left side of the chamber and aimed towards the substrate housing. The chamber must be filled with 2mTorr of nitrogen gas in order for the gun to operate properly. The ion gun works by emitting electrons from a cathode filament, causing the nitrogen inside the gun to be positively ionized. These electrons are directed in a circle inside the cylindrical gun due to the magnetic field produced by magnets placed on either side of the housing so that they have a greater probability of colliding with an atom and ionizing it. The ions are then accelerated outwards toward the substrate by the negative voltage on the grid which is $\sim 250\text{V}$. A separate current is run through the neutralizer filament causing it to emit electrons. The electrons are repelled by the negative voltage on the grid, thus they are also accelerated outward towards the substrate. The electrons counteract the positive ions, thereby causing a neutrally charged beam of nitrogen ions and electrons incident on the substrate to remove contamination atoms on the surface through the transfer of energy while keeping the substrate from having an imbalance of charge which could affect the samples.

3.2.3 Evaporation System

The five crucible evaporation system has a filament, located beneath the hearth, which emits electrons while a magnetic field, created by the magnets in the hearth, directs the electrons around in a circle to strike metal source pellets which lie in isolated grounded crucibles as illustrated in Figure 14. The energy of the emitted electrons is transferred to the pellets, thus melting and then evaporating them into the chamber. Because this beam is focused, only the metal source becomes hot and the rest of the system stays relatively cool. To ensure heat reduction, the evaporation hearth has an internal hydro-cooling system. The shields reabsorb stray electrons from the filament, which is located under the hearth to prevent evaporated particles from interfering with the electron beam.

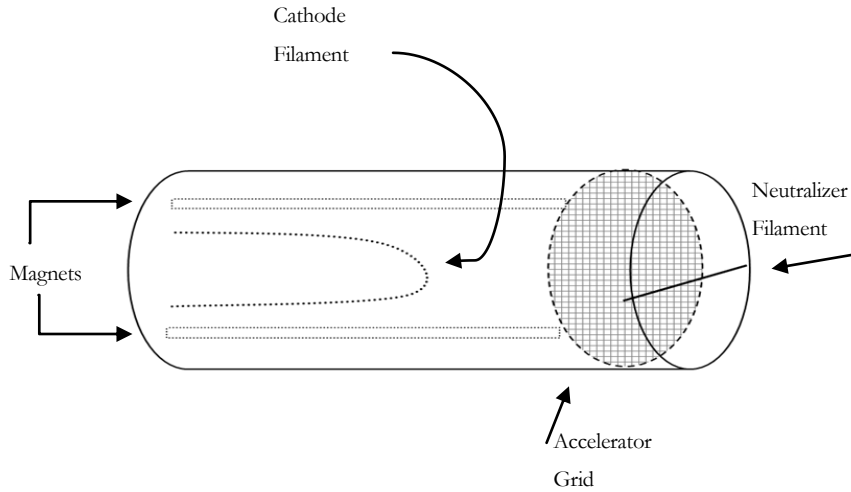


Figure 13. Diagram of ion gun, the cathode filament emits electrons which ionize the Nitrogen gas in the chamber. The grid accelerates the ions through it towards the substrate. The particles of contamination on the substrate will be removed by the momentum transferred from the ions (at collision). The neutralizer filament emits electrons that counteract the positive ions so that the substrate is not imbalanced.

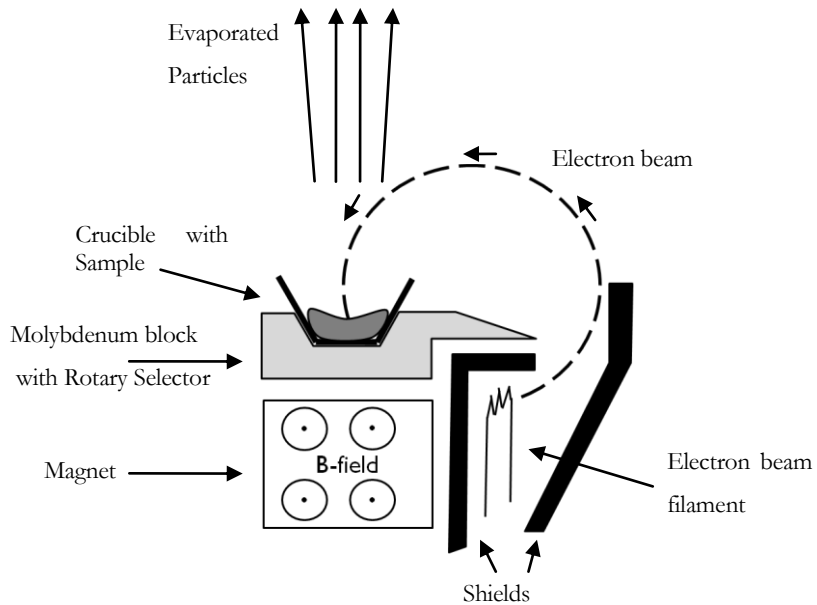


Figure 14. The evaporation system consists of a hearth constructed from molybdenum, which has an extremely high melting point thus reducing the chance of contamination of the sample. The construction of this system keeps all parts below the hearth thereby allowing the evaporated particles to scatter straight up to the rest of the chamber, specifically to the substrate.

The rotary crucible selector which is connected to the end of the hearth is attached to a rotary feed through, which allows it to be accessed outside of the chamber. This enables the crucibles to be changed while the system is still pumped down; therefore allowing the construction of a metal film of different kinds of layers.

3.3 Profilometer

After the films have been constructed it is necessary to measure the film thickness so that the dependence of film orientation on the thickness can be assessed. The Alpha-Step 500 profilometer is used to determine the thickness of the films. A DOS operating system computer controls the profilometer tray and needle position. The substrate is placed film side up inside the housing (which was not under vacuum) on the tray, which is then raised until the needle is just touching the film, thereby calibrating the height. The needle displacement corresponds to the thickness variation of the surface of the sample, which is used to identify the thicknesses of silver and titanium relative to the substrate. There are two knobs outside the housing connected to the tray which move the tray laterally to any horizontal or vertical position of the sample to allow the general location of the reading to be controlled. To take a scan, the operating system moves the needle horizontally from left to right at a specifiable rate and position, measuring the change in needle height at a specifiable rate. The rate can be chosen depending on the thickness and quality of the sample to ensure a good reading. After calibrating the height to a flat reference surface, the needle displacement as it corresponds to the position is plotted graphically; thus the data is returned as a two dimensional plot of needle height verses horizontal position of the needle.

3.4 Annealing Furnace

The annealing system, shown in Figure 16, uses a Marshall Two-Zone Furnace to heat the contents of a glass tube to temperatures up to 600°C and a portable vacuum pump system which has a roughing pump which will bring the pressure of the tube down into the 10^{-3} torr range and a turbo pump allowing the tube to reach pressure on the magnitude of 10^{-5} torr. The Nitrogen Flow Controller system is used in conjunction with the above apparatus to aid in thermal conduction, as detailed below.

Sample pieces are placed inside under vacuum in the glass tube which can freely slide horizontally in and out of the furnace. The end of the tube has a three way connector that allows the chamber of the

tube to be connected to either the vacuum system or the nitrogen gas flow. First the vacuum pump station can be used to pump down the tube and remove atmospheric contamination, after which the valve to the vacuum can be shut and the valve to the nitrogen opened. The gas flow allows the internal contents of the tube to reach the external temperature faster than when the tube is under vacuum through convection. The furnace can be manually heated to the desired annealing temperature, which is monitored by the thermocouple wire running to the same location in the tube as the samples. After the tube is flooded with 1atm nitrogen gas, the tube is moved inside the furnace for a determined period of time. Thus the samples are annealed for any desired length of time in a clean environment.

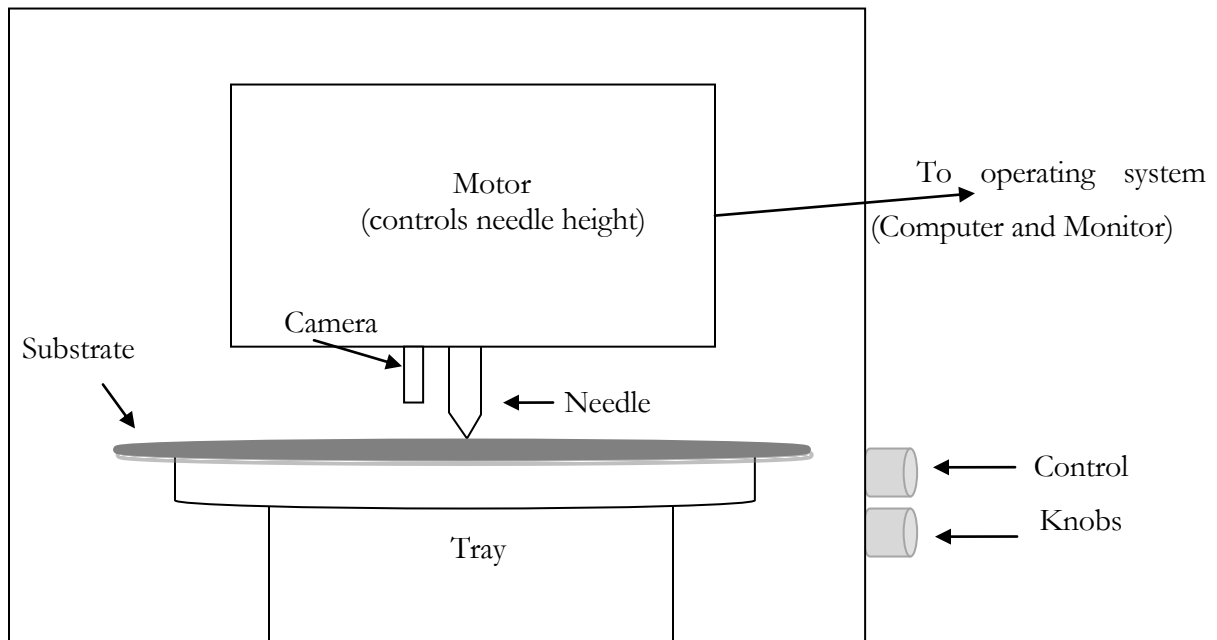


Figure 15. Diagram of profilometer, the substrate is placed film side up on the tray and the needle is lowered until it just touches the film. The user can control the initial placement of the substrate with the control knobs (that move the tray) and the operating system controls the movement of the needle (from left to right) for each scan. The profilometer can measure the height difference and output that height as it corresponds to the horizontal position on the substrate.

3.5 Passivation Chamber

The sputtering chamber used to deposit the passivation layer on top of the evaporated films is located in the Cornell Nanoscale Facility (CNF) and has the capacity to deposit four different metals, which can be switched while the chamber is pumped down. The lowest pressure of the chamber is on the order of 10^{-7} torr and a gas flow valve allows the chamber to be operated under a higher pressure Argon gas atmosphere, on the order of 10^{-4} torr. The metal source to be sputtered is placed in the top of the chamber.

The Argon gas, once ionized, creates a plasma from which individual ions are accelerated to collide with the source (held at a high negative voltage) causing particles to be sputtered down onto the substrate through a slit. The substrate is continually rotating so that each time it passes underneath the slit it receives one layer of sputtered material. The thickness of the film depends on the rate of sputtering and rotation.

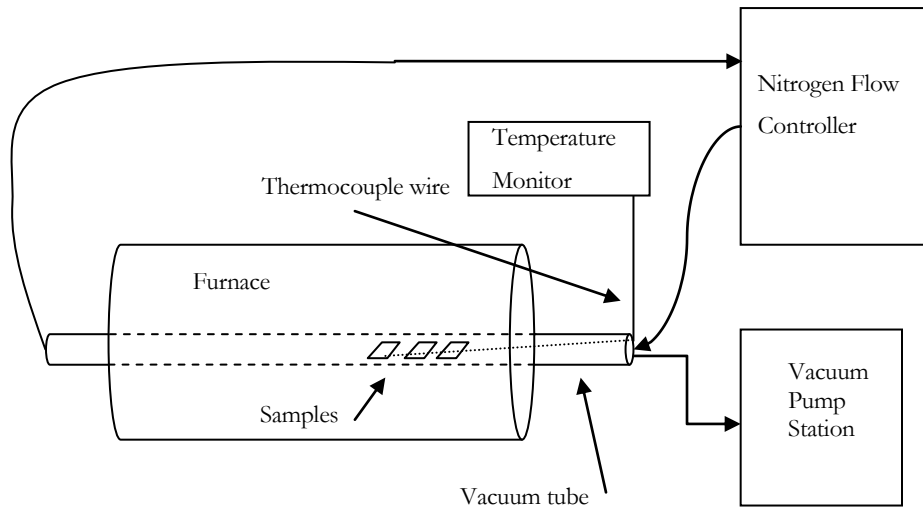


Figure 16. Diagram of Annealing Furnace. The furnace has two internal cylindrical heaters (not shown) that are side by side and can be ramped up manually or automatically. In the center of the furnace is a small cylindrical hole in which a glass tube can be placed and the temperature of the contents will be increased through radiant heating. The Nitrogen Flow Controller and Vacuum Pump Station

can be attached to the end of the tube (independently) to allow either an atmospheric pressure flow of nitrogen through the contents or keep the contents under low pressure.

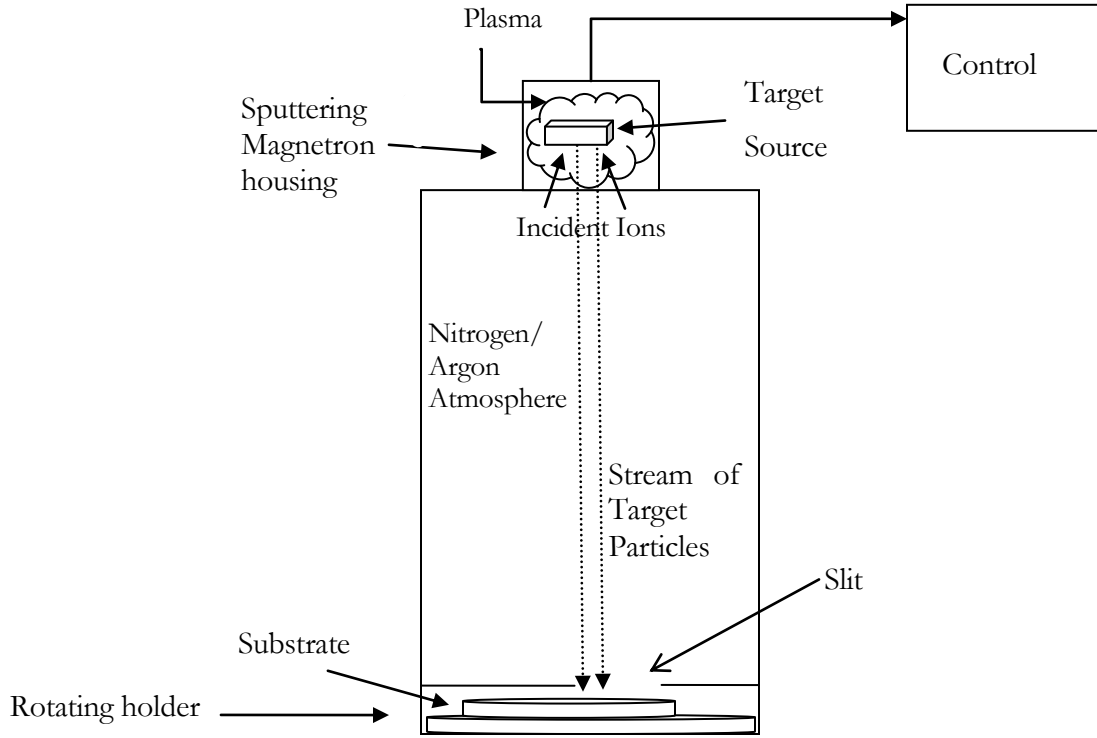


Figure 17. Sputtering chamber used to passivate samples. The Argon atoms are ionized by the electrons that are freed from the target when the target is placed at high negative voltage. The ions create a plasma which is sustained by the magnetron because the magnetic field keeps the secondary electrons (emitted from the Argon) circling in the plasma. Having all these process on the top of the chamber allows the ions to collide with the target, transferring momentum and enabling atoms of the source to project onto the sample, while reducing the risk of contamination.

3.6 X-Ray Diffractometer

The Scintag PAD-X theta-theta diffractometer (Figure 18) used to acquire the film orientation data functions by projecting x-rays from the x-ray source at a specific angle onto the sample placed in the center of the apparatus. The incident beam size is 1.0 mm by 10 mm, and the spot size of x-rays on

the sample holder is always 10 mm wide, but the length varies (depending on the angle and collimating slit size). The reflected x-rays are then received into the solid state germanium detector and the number of the x-rays scattered at different diffraction angles are counted. The number of counts as determined by the detector is then relayed to a computer. The rotation mechanisms are each separately marked from 0° to 360° about the entire circumference and the x-ray tube is attached to the inner one and the detector to the outer one. Each time the diffractometer is turned on, the system must be calibrated by observing the angles above the horizontal at which the x-ray tube and detector are sitting and entering that value into the computer. Then the computer can calibrate the diffractometer by adjusting both to zero. The computer controls the motion of both rotation mechanisms and allows the x-ray source and detector to simultaneously rotate about the source in opposing directions. Thus a range of angles can be scanned for each collection of data, and the angle above the horizontal will be the same. Also a specific range of angles can be programmed into the computer allowing for a selection of specific angle ranges to be scanned. The x-ray tube and the detector are secured to the rotation mechanisms so that the distance from either of them to the center of the sample holder is always 250 mm.

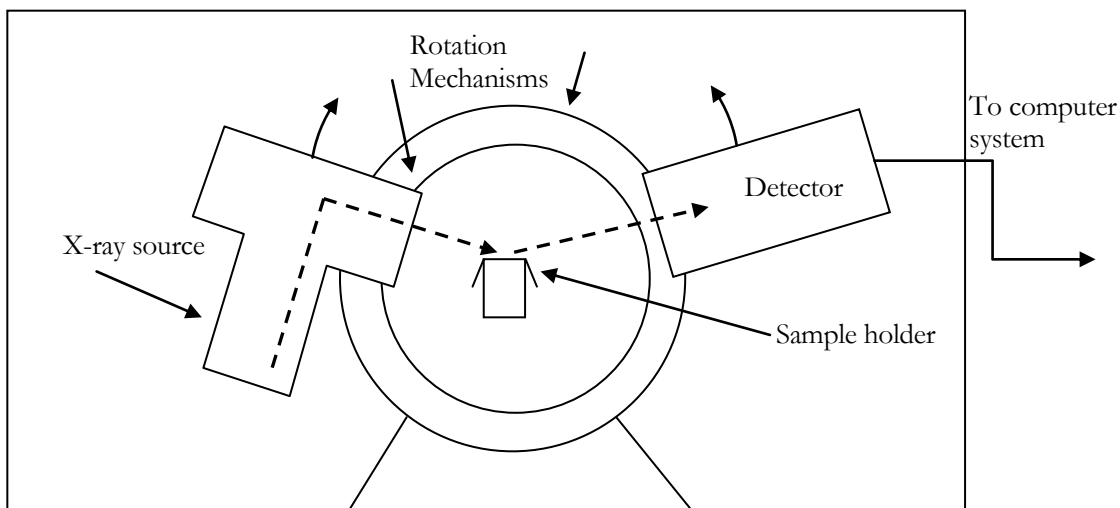


Figure 18. Scintag x-ray diffractometer, the sample holder in which the films are placed for analysis is in the center of the rotation mechanisms. Attached to the rotation mechanisms are the x-ray tube and the detector which are simultaneously rotated about the sample to maintain the same angle above the horizontal.

Chapter 4

PROCEDURE

4.1 Deposition Process

The films were deposited on 100mm diameter circular silicon substrates that were p-doped and had a 50 nm thick layer of nitride on the top side which was deposited on. In order to determine the thicknesses of the films a ~3 mm thin strip of metal was secured along the center of each substrate to keep any particles from depositing on that section of it.

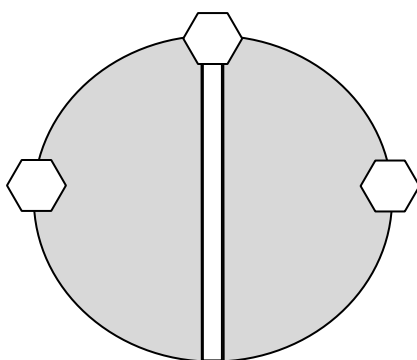


Figure 19. Silicon substrate with metal strip placed down center, allowing the bare substrate to act as the zero point for measuring the thickness. The three screws as shown held the substrate in place on the sample holder (not shown) and the holder rested on similarly placed bolts at the top of chamber.

The substrate was attached to the sample holder and the holder was placed at the top of the deposition chamber. It was secured by a wire to three bolts it rested on that were attached to the ceiling of the chamber. Before the lid was lowered to begin pumping down the chamber, any surface that may have been contaminated with fingerprints was wiped with ethyl alcohol and methanol and the crucibles were filled up with pellets of the metal necessary to make the desired film. The system needed approximately four to five hours to reach vacuum levels of 10^{-6} torr and once the ion gauge read that value or lower, the substrate was ion cleaned in prepared for deposition.

4.1.1 Ion cleaning

The ion cleaning removes a negligible layer, on the order of a few nanometers, from the substrate. The rotary motor was turned on to ensure that a uniform layer was removed. The linear shutter was moved to the back of the chamber (so as not to block the substrate) and the rotary shutter was placed over the substrate so that when the ion gun was turned on particles would not be removed while the settings were being adjusted and set. The valve to the nitrogen gas was opened and after the pressure, as displayed on the ion gauge, increased to $2 \cdot 10^{-4}$ torr, (which indicated that the chamber was flooded with gas) the ion gun was turned on and the currents to the filaments were raised. The standard beam current and voltage were 14 mA and 250 V respectively and the period of substrate exposure was 100 seconds. Then the nitrogen flow was turned off and the residue gas pumped out of the chamber so the system returned to high vacuum for the remaining duration of the deposition process.

4.1.2 Film Deposition Processes

The following sections describe how the substrate and shutters were aligned in various ways so that the film could be layered and the thickness varied to deposit the desired combination on each substrate.

4.1.2.1 Films with Silver

To make a film of one type of metal that has a thickness gradient, both shutters were moved into position covering the substrate. The linear shutter was programmed to move across the entirety of the sample at a constant rate and the evaporation system was turned on. When the correct evaporation rate was reached, simultaneously, the rotary shutter was moved completely away from blocking the substrate and the linear shutter started along its specified path. After deposition was completed the rotary shutter was moved back into place, covering the sample, and the evaporation system was promptly deactivated.

4.1.2.2 Films with Silver and Titanium

Making a film that has two layers of titanium required a combination of the above two procedures. Titanium films were deposited both on top and below the silver film. To construct this type of film, first a constant layer of 50 nm of titanium was deposited, then the evaporation hearth was adjusted to

deposit silver with a gradient procedure, and then the hearth was moved back into place to make a third uniform layer of 50 nm of titanium on top. There were some samples in which titanium layers were deposited on only half of the sample so that the effect of titanium could be compared to silver gradients at identical thicknesses, see Figure 21.

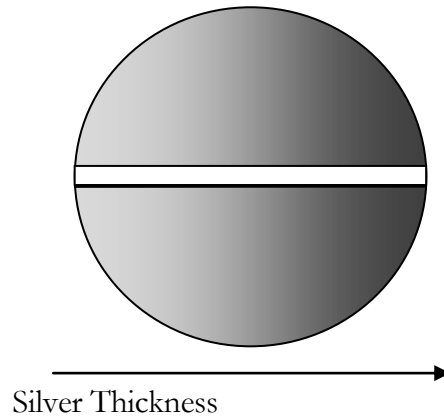


Figure 20. This diagram represents a silver film with a thickness gradient that parallels the strip down the center of the substrate.

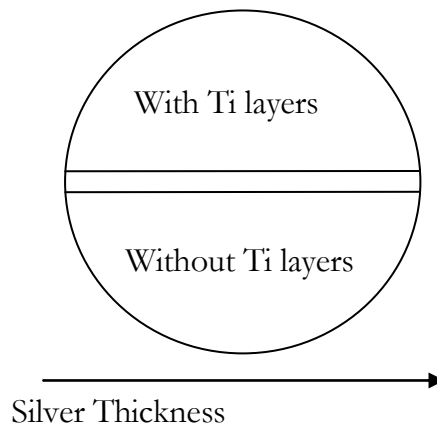


Figure 21. Silver gradient with half of the substrate including titanium layers both on top and below the silver film.

This required the sample to initially be rotated so that the protective strip was parallel with the linear shutter, which was moved forward so that half the substrate was covered during both titanium depositions. For the silver gradient deposition, the sample was turned another 90 degrees so that the strip was perpendicular to the linear shutter, and then turned back for the last layer.

4.1.2.3 Silver and Titanium with Two Gradients

In order to have a film with gradients of both silver and titanium the above process of sample rotation was used, but the linear shutter was programmed for an additional gradient over the entire sample instead of just covering half of it. This gave the sample two gradient films perpendicular to each other, as shown in Figure 22. This creates a substrate that has each possible thickness combination of the silver and titanium.

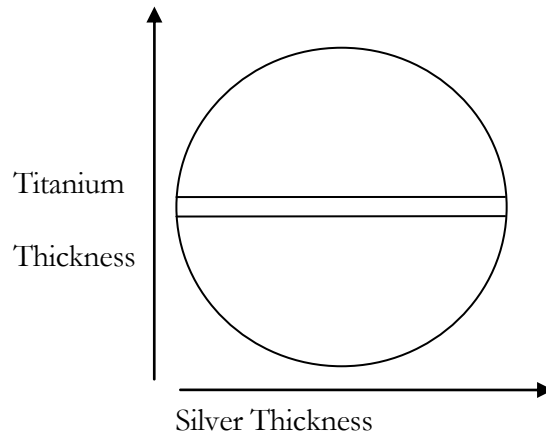


Figure 22. Silver and titanium with perpendicular gradients.

4.2 Profilometry

To measure the thickness of the film each substrate had a horizontal ~3 mm wide strip of bare substrate along its entire length. During deposition, that area was covered; thus after the film has been deposited the cover was taken off, yielding a permanent step across the substrate from film to substrate. The center strip was scribed by hand at vertical 5-10 mm increments so that the thickness data could be referenced and used to extrapolate a plot of the thickness verses position on the substrate.

Setting the scanning distance (horizontally across the film) to 300-500 μm and the rate of the needle to 10-20 $\mu\text{m/s}$ were experimentally determined to yield the best results. Scans were taken on either side of the bare strip, at each etched point. On the monitor, the view from the camera was shown and thus details of the film could be seen. This meant that large deformations could be avoided when picking a place to take a scan. After a scan was taken, the data needed to be leveled or calibrated so that the computer program had a reference point to determine what was perpendicular to the thickness measurements. The scans were consistent to each other to within a range of ± 50 nm, so this was the approximate error in the thickness measurements.

Measurements that were not calibrated to the top of the silver had the tendency to go out of the scanner's range and had to be re-measured accordingly. For thicker silver films on the order of ~ 3 μm , it was advantageous to begin with the tip touching the substrate, so that the scanner did not drop out of measurable thickness range by going too high or low.

After acquiring the thickness data, the position of each measurement was mapped out by a thickness of silver verses position on the substrate with a line plot. The two thickness measurements on either side of each etch were averaged and a trend line plotted to yield an equation that represents the entire gradient. From this the actual deposition rate was calculated for deposition calibration purposes and the thickness (along the vertical gradient) of any point on the substrate was estimated. The deposited thickness was estimated as being horizontally uniform across the entire width of each sample due to the fact that there was no reliable technique available to directly measure the thickness of the film anywhere besides the middle section.

4.3 Passivation

After the thickness was measured, a passivation layer of approximately 50 nanometers of aluminum nitride was sputtered onto the film. Samples were placed inside the sputter deposition chamber on the rotary base, with the strip oriented so that it was pointing in the direction of rotation. The rotation rate for the sample was set to 20 rpm.

Prior to deposition, the sample was ion cleaned. As most samples had thin titanium films on top, the known rate of thickness removal (23 $\text{\AA}/\text{min}$ of SiO_2 or 16 $\text{\AA}/\text{min}$ of silicon in an argon atmosphere of

1.6 mT, where the standard time is 3-5 minutes) indicated that one minute of ion cleaning time was sufficient. Longer times would lead to significant and undesired erosion of the titanium film.

The passivation layer of 99.995% elemental aluminum was magnetron sputtered in a nitrogen/argon atmosphere of 20 sccm N₂ and 10sccm Argon at 4 mTorr pressure. Prior experimentation yielded a deposition rate of $\sim 33\text{\AA}/\text{min}$, so 15 minutes of deposition was the time used to obtain ~ 50 nm of aluminum nitride.

4.4 Annealing

Post-passivation and pre-annealing, the substrate was scribed and labeled in a grid form and broken into columns that fit in the annealing furnace tube. After annealing they were broken into squares, for x-ray diffraction, that were approximately 100 millimeters square.

First the samples were placed in the tube and the three way connector was attached to the end. In vacuum, the thermal transfer was limited to the contact of the heated tube and radiation. To control the temperature inside the tube, the tube was evacuated with a roughing pump and then flooded with 1 atmosphere of nitrogen. The roughing pump removed a majority of the airborne residue and contamination then, because the tube was filled with nitrogen, there was no need for further evacuation (which could be done with the turbopump component of the station). A slow rate of nitrogen passed through the tube and out the valve on the other side, which was opened after the valve to the roughing pump was closed. The gas then bubbled through a beaker of water, and therefore the rate of nitrogen flow was monitored by the intensity of bubbling in the beaker and the rate was controlled by a mass flow regulator.

The furnace had its own temperature display, but the monitors were outside the vacuum tube, thus a thermocouple wire inserted directly into the tube under the oven and directly over the samples yielded more accurate temperature readings. The furnace had a programmable ramping ability but had a time delay which would cause the temperature to rise beyond the programmed maximum temperature. Thus the power was best adjusted manually to accurately control the temperature of the furnace.

The most efficient process was to preheat the oven and then after the oven had reached the desired temperature the tube containing the samples could be slid in and out of the oven while it was filled

with flowing nitrogen. Samples were held at a constant temperature for one hour and then after the anneal was complete, the tube was pulled out of the oven and allowed to cool to room temperature while still under Nitrogen flow.

4.5 X-Ray Diffraction

After the samples were broken into squares each piece was analyzed through x-ray diffraction. The sample holder held one piece at a time and sample pieces were placed in the center of the tray on an insulated platform. Shims that were the same height as the sample were used to keep the sample even with the tray's original depth, as shown in Figure 23.

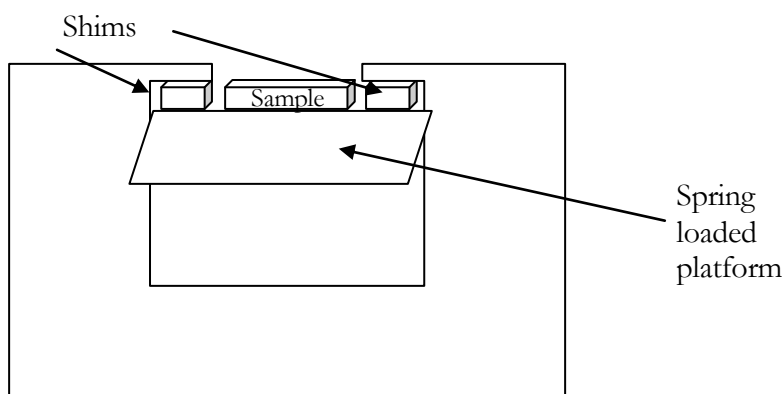


Figure 23. The diffractometer sample holder, the platform had a spring (spring not shown) which compressed the platform against the holder. The shims kept the top of the sample at the original height of the platform.

The standard operating voltage and current of the diffractometer were 45 kV and 40 mA, respectively. The diffractometer had collimating slits that allowed the beam width and intensity to be controlled. Smaller slits for both the x-ray tube and detector were used to limit the number of counts because the detector has a maximum rate at which it can measure an accurate count of the number of x-rays that are reflected. Thus if the maximum rate was exceeded the output of the detector will yield a lower number of counts than what was actually reflected. So for this detector any data collected that resulted in ~30,000 (or more) counts per 0.24 seconds needed more restrictive slits or settings. The slits used in the x-ray tube were 1 cm and 3 cm and the slits on the detector were 0.1 cm and 0.3 cm. The scans

ranged over the angles of 36°-46° at 5-6 deg/minute which took approximately 2 minutes. The samples with titanium had much stronger intensity measurements than those with just silver, thus the power settings were reduced to 20 kV and 15 mA for those samples. The data processing program fit the measured number of counts to Pearson-7 curves and the relative areas under the curves were determined for each angle peak.

Chapter 5

ANALYSIS AND RESULTS

5.1 Introduction

It was concluded that placing Ti layers on either side of the silver film did have an effect on the orientation transition. Also, experimentation with the annealing temperature and the quantity of annealing time showed that the transition could be controlled. Each two dimensional data plot is of the volume percent of (111) verses the thickness.

5.2 Preliminary Results

Figure 24 shows the expected transition from (111) to (100). However, when the model (Figure 7) is compared to the data, the measured transition of the data is clearly less steep. Titanium, an adhesion promoter, had the potential to affect the transition so the subsequent films were deposited with titanium to observe any differing results.

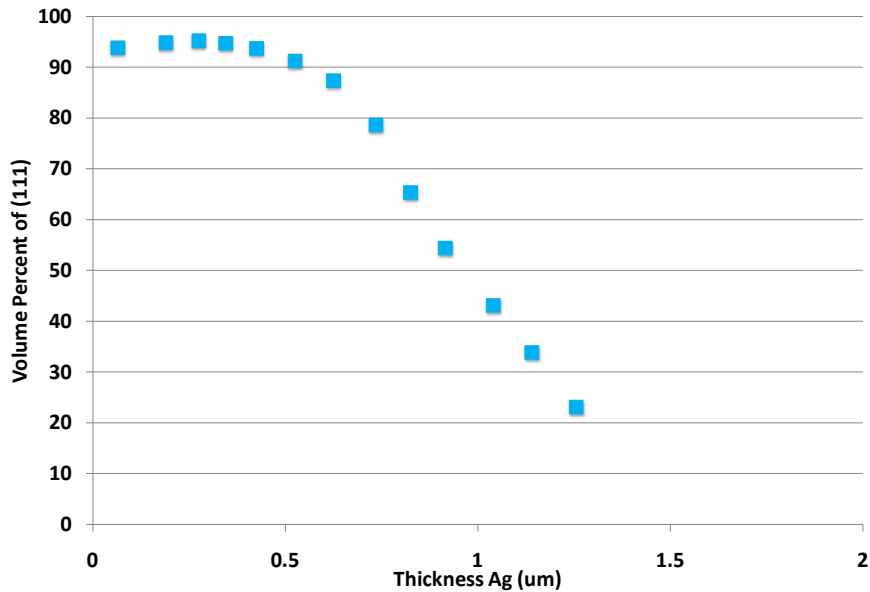


Figure 24. Preliminary data plot of a silver film ranging in thickness from zero to ~1300 nm, observe the gradual transition.

5.3 Titanium Effects

The concept of placing an adhesion promoter on either side of the silver film was implemented to yield Figure 25, where the titanium and silver layers were deposited in perpendicular gradients. From this sample it can be seen that the orientation transition is sharper for the films that had thicker layers of titanium. Also, the thickness of titanium layer itself was a factor in the steepened transition.

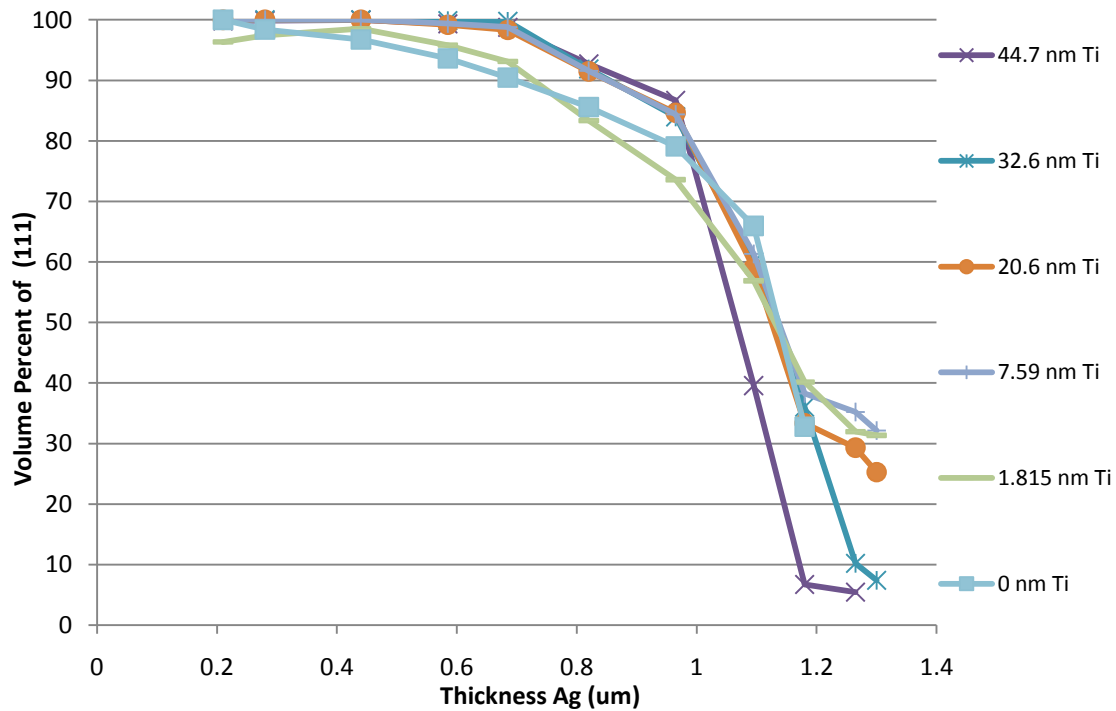


Figure 25. Comparison of film data that has titanium layers of various thicknesses. All samples in this plot were annealed at 260°C. Comparing the film with 44.7 nm of titanium to the film with no titanium, it can be seen that the thickness range (from where the transition begins to where it finishes) is less for the film with 44.7 nm of titanium.

From this data it was observed that there is a difference between the thickness range of the orientation transition. When titanium layers were placed on either side of the thin film then the thickness range, from when the film begins transitioning from 100 percent (111) to when it reaches 100 percent (100) was reduced.

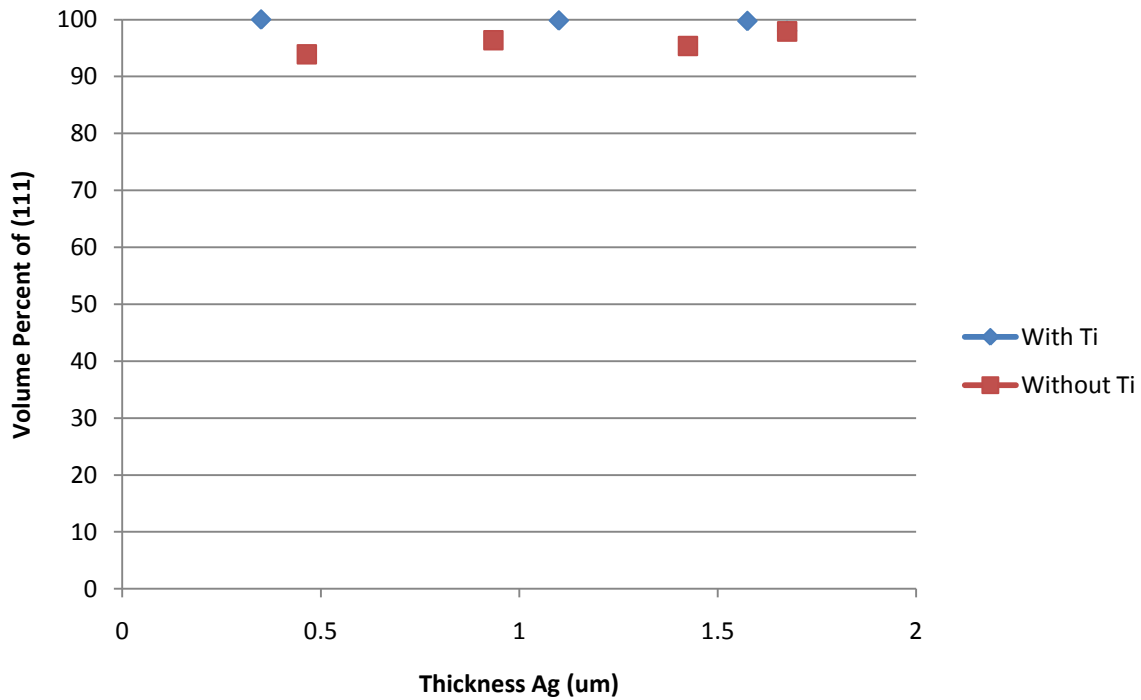


Figure 26. Analysis of sample that was taken pre-passivation and pre-anneal (as deposited).

Observation of the data in Figure 26, shows that there was a small percentage of silver films that was deposited as (100). However, when titanium layers were deposited the film contains much less (100) orientations, and appears to be 100 percent (111).

5.4 Annealing Effects

Films were initially annealed at $\sim 500^{\circ}\text{C}$ for 2 hours, which resulted in the transition as shown in Figure 25. Comparison of film data that has titanium layers of various thicknesses However, the minimum temperature or time necessary to achieve the full transition was unknown. To determine those conditions, the length and degree to which the films were annealed was varied and the resulting data was analyzed. It was noted that the temperature reached during passivation was estimated to be a maximum of 120°C briefly, which possibly affected the grain growth and transformation, but diffraction analysis done pre and post passivation, showed a negligible influence.

5.4.1 Annealing Temperature

To observe the transition under different annealing temperatures, samples of the film that had the same thickness ranges were annealed at various temperatures. Thus all the factors of each data set were constant except for the temperature, thereby enabling the influence of temperature, on the orientation transition, to be observed.

It can be seen that after deposition and before annealing the film was primarily (111) oriented over all thicknesses. As the annealing temperature increased over a constant period of one hour, the volume of (100) orientations increased. Also, the thickness of silver at which the transition is completed decreased.

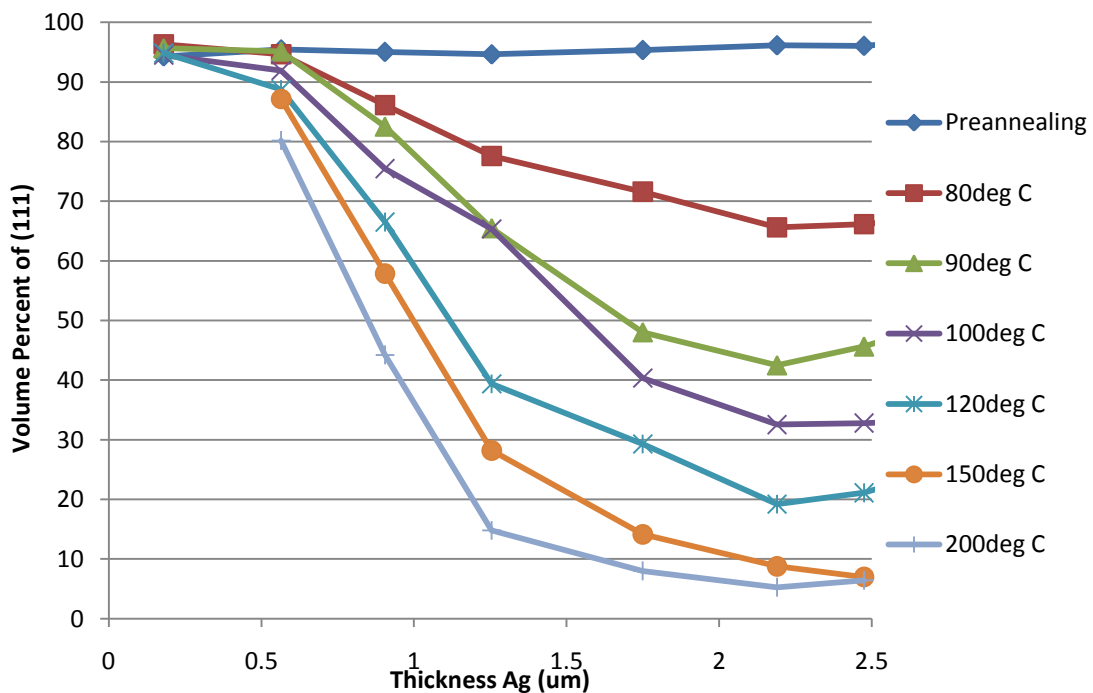


Figure 27. Silver film without titanium layers annealed for 1 hour at varying temperature. Note that as the temperature increased the transition became more defined.

The same process was completed with a silver film that had layers of titanium; see Figure 28. Notice that for lower temperatures, the film began transitioning but at thicknesses greater than $1.5 \mu\text{m}$ the volume that changed orientations to (100) was much less. This seems to imply that thicker films require more thermal energy to transition from (111), because at lower temperature there is less energy. As the temperature was increased the transition to (100) increased, similar to the transformations seen in Figure 27. The slow transformation of the silver and titanium films annealed under lower temperatures led to experimentation with the length of annealing time.

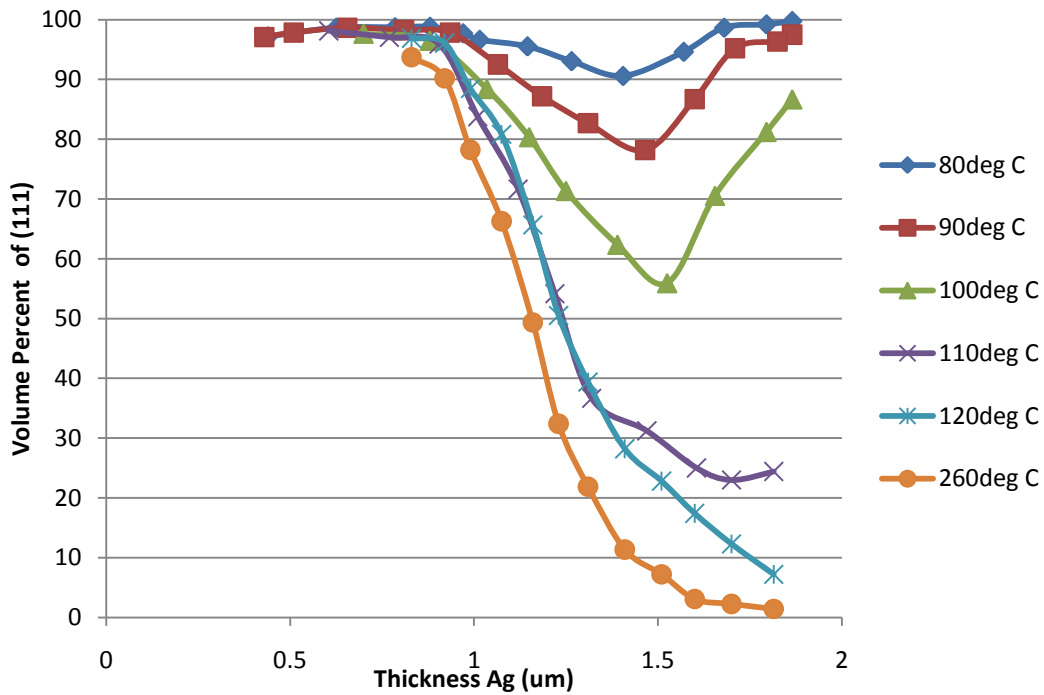


Figure 28. Silver film with titanium layers annealed for 1 hour at varying temperatures. Again, after the temperature increased the films transformed further.

5.4.2 Annealing Time

To determine the behavior of the film at low annealing temperatures the length of time for a given data set was progressively increased and x-ray diffraction analysis was taken after each anneal.

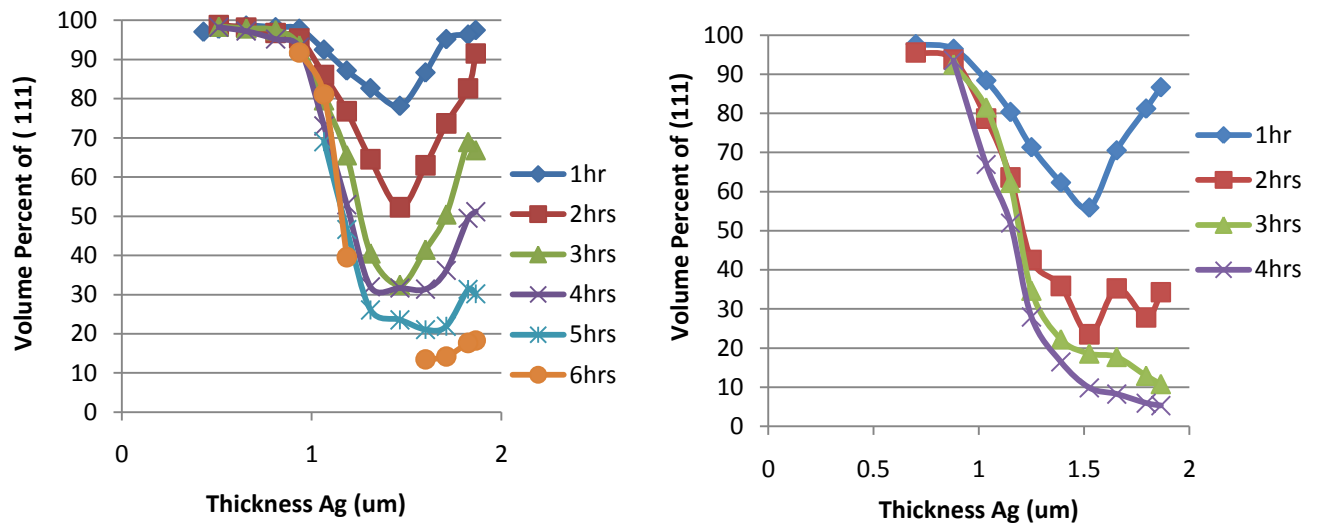


Figure 29. Silver films with titanium layers annealed for increasing periods of time. On the left the temperature was held constant at 90°C and on the right the temperature was held constant at 100°C. Samples were re-annealed for 1 hour to supply data for subsequent hours.

This was done for temperatures of both 90°C and 100°C. The film annealed at 90°C needed to be annealed for six hours before it fully transitioned; however, the film annealed at 100°C only needed four hours before it reached the same transition point. From the data in Figure 29 it can be determined that the full transition to (100) for these lower temperatures does occur after extended anneal time.

Chapter 6

CONCLUSIONS

6.1 Summary

It could be seen that placing layers of titanium on either side of the silver film caused the film to have different orientation transition behavior when compared with films which were constructed with only silver. In conclusion, it can be concluded that titanium sharpens the transition from (111) orientations to (100) orientations. In addition, the thickness range in which the transition takes place is reduced. The thickness of the titanium layer itself appeared to increase in influence of the transition with increased thickness. Useful further experimentation would be to determine the thickness threshold point, after which increasing the thickness of the titanium films would have no effect. It can also be observed that for the majority of the data taken, the transition took place at a thickness of $\sim 1\mu\text{m}$.

The effects of the annealing temperature and time were measured to observe and determine the minimum of each required to drive the full orientation transition to (100). From the results it can be concluded that if the temperature was reduced, the transition would still occur when the annealing time was increased. Likewise, the time could be reduced when the temperature was increased. Furthermore, increasing temperature seemed to be more of an influence to the transition than increasing annealing time. Thus by controlling these factors the transition could be controlled and determined.

It was noted that when silver films were deposited, there was a percentage of the film that was deposited as (100), but when titanium layers were deposited before and after the silver film, there was no (100) orientation in the film immediately post-deposition. The reason behind this behavior has yet to be determined and is an area for further study.

6.2 Further Analysis

Another aspect for data analysis is measuring the curvature in thin silver films. Curvature is caused by the strain in films, where the strain is correlated to the grain orientations within films. By measuring the strain in the films a more detailed model can be developed of how the strain energy effects the

orientations. When films have been strain tested, the microstructure, as determined from the x-ray diffraction analysis, can be compared with the strain energy for any given sample of film.

6.3 Imaging

In future work, the films could be observed through equipment that would result in images of the films. There are four methods that could be used to observe thin films. The four methods are: focused ion beam (FIB) imaging, transmission electron microscopy (TEM), scanning electron microscopy (SEM) and electron backscattering diffraction (EBSD). Strain testing and x-ray diffraction yield averages of film grain orientations. However, the images obtained via these methods result in specific details such as size and shape of the grains or images of grain boundaries.

TEM, SEM, and EBSD all employ the use of an electron beam to create an observable image of the microstructures in the thin film, as opposed to the ion beam utilized in FIB. With SEM the electron beam interacts with the atoms in the film and it is primarily the secondary electron signal that forms the image. In EBSD, the diffracted electrons produce an electron backscatter pattern, which is a direct mapping of the crystal orientations. TEM and FIB result in images that are high resolution and show a profile of the sample. It can be determined from observation of the grains from the side whether the grains in the sample are random (growing in no predictable or repeating pattern) or columnar (growing in columns). The information and data acquired through these methods could confirm the determined conclusions and possibly answer the questions raised by the experimental results.

REFERENCES

- [1] L.B. Freund and S.Suresh, *Thin Film Materials* (University Press, Cambridge, 2003), p.xvi.
- [2] D.L. Smith, *Thin Film Deposition* (McGraw-Hill, Inc., New York, 1995), p. 2.
- [3] Y. Zoo and T.L. Alford, J. Appl. Phys. **101**, 1 (2007).
- [4] R-M Keller et al. J. Mat. Res.**13**, 1307 (1998).
- [5] S. Hosokawa *et. al.* in *AIP Conference Proceedings, 2007*, p. 1309.
- [6] H.S. Ullal, National Renewable Energy Laboratory CP-540-42058 (unpublished).
- [7] I. Lau *et. al.* Molecular Structures & Liquid Crystals. **446**, 1 (2006).
- [8] M.J. Kobrinsky and C.V. Thompson, Appl. Phy. Lett. **73**, 17 (1998).
- [9] B.D. Cullity, *Elements of X-Ray Diffraction* (Addison-Wesley Publishing Company, Inc., Reading, 1967), p. 215.
- [10] L.B. Freund and S.Suresh, *Thin Film Materials* (University Press, Cambridge, 2003), p. 6-7
- [11] D. M. Mattox, Handbook of Physical Vapor Deposition (PVD) Processing. (Noyes Publications, Park Ridge, New Jersey, 1998), p. 5,6, 9
- [12] W.H. Zachariasen, *Theory of X-Ray Diffraction in Crystals* (Dover Publications, Inc., 1945), p.3-4.
- [13] Y. Zoo and T.L. Alford, J. Appl. Phys. **101**, 1 (2007).
- [14] L.B. Freund and S.Suresh, *Thin Film Materials* (University Press, Cambridge, 2003), p. 61.
- [15] *The Strain Gauge*, Transactions in Measurement and Control **3** (2010).
- [16] C.V. Thompson and R. Carel, Mat. Sci. Eng. **B32** (2005).
- [17] Baker, Saha, Lin, and Shu, Unpublished.
- [18] D.L. Smith, *Thin Film Deposition* (McGraw-Hill, Inc., New York, 1995), p.382.
- [19] B.D. Cullity, *Elements of X-Ray Diffraction* (Addison-Wesley Publishing Company, Inc., Reading, 1967), p.80, 82.
- [20] D.L. Smith, *Thin Film Deposition* (McGraw-Hill, Inc., New York, 1995), p.248-249.
- [21] B.D. Cullity, *Elements of X-Ray Diffraction* (Addison-Wesley Publishing Company, Inc., Reading, 1967), p.82.